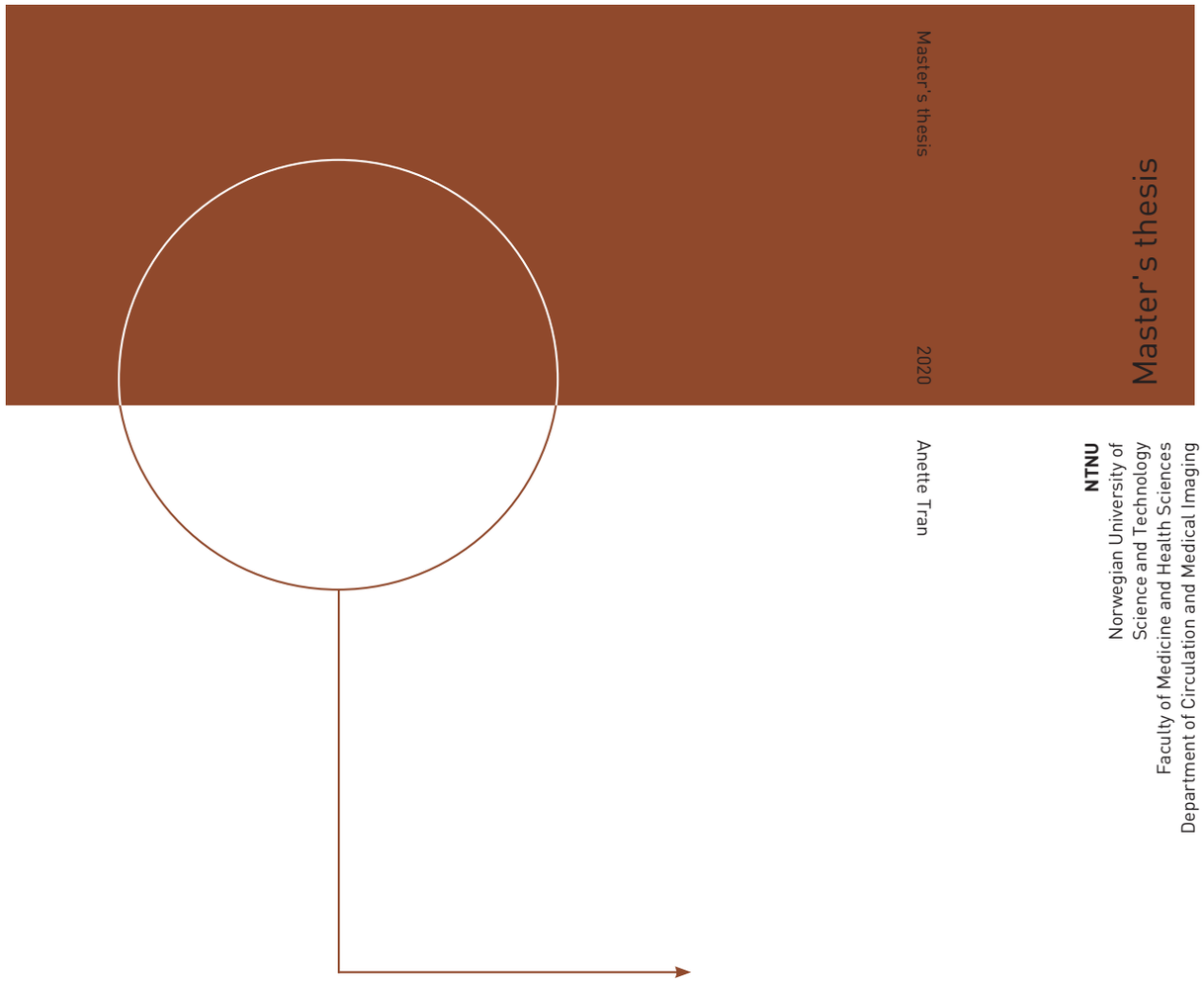

Master's thesis

2020

Anette Tran

NTNU
Norwegian University of
Science and Technology
Faculty of Medicine and Health Sciences
Department of Circulation and Medical Imaging

Anette Tran

Effects of hypoxia/reoxygenation and miR-24-3p in human cardiomyocyte models

June 2020

NTNU
Norwegian University of
Science and Technology

NTNU
Norwegian University of
Science and Technology

NTNU

Norwegian University of
Science and Technology

Effects of hypoxia/reoxygenation and miR-24-3p in human cardiomyocyte models

Anette Tran

MSc in Molecular Medicine
Submission date: June 2020
Supervisor: Dr. Morten Andre Høydal
Co-supervisor: Dr. Nathan Robert Scrimgeour

Norwegian University of Science and Technology
Department of Circulation and Medical Imaging

Abstract

Background: Effective cardioprotective therapies targeting the reperfusion phase of ischemia/reperfusion (I/R) injury are lacking, which remain one of the top unmet clinical needs in cardiology. MicroRNAs (miRNAs) are a class of small non-coding RNAs that regulate proteins at the post-transcriptional level. These molecules have recently been recognized as key players in the progression of heart disease. From previous data collected by the Group of Molecular and Cellular Cardiology at NTNU, miR-24-3p was found to be significantly upregulated in patients with post-MI HF. This miRNA has been found to target BIM, a pro-apoptotic member of the BCL-2 protein family. Therefore, we hypothesized that miR-24-3p may potentially have cardioprotective effects relating to apoptotic cell death. Technologies such as multi-well microelectrode arrays (MEAs) enable non-invasive recording of field potentials (FPs) of electrically active cells *in vitro*. This makes it possible to study the electrophysiological properties of human induced pluripotent stem cell-derived CMs (hiPSC-CMs), which closely recapitulate the function of native CMs *in vivo*. Taken together, the aims of this thesis were to (1) assess the temporal electrophysiological changes hiPSC-CMs exposed to *in vitro* I/R-simulated environments; (2) investigate potential cardioprotective effects of miR-24-3p-specific mimics and inhibitors on hiPSC-CMs in these environments; (3) verify the functional output from the hiPSC-CMs with molecular assay data collected from AC-16 CMs, an immortalized cell line fused with primary adult ventricular CMs.

Methods: A MEA system was used to record FPs of hiPSC-CMs in real-time. hiPSC-CMs and AC-16 CMs transfected with miR-24-3p-specific mimics and inhibitors were subjected to 18h hypoxia (1% O_2) and 4h reoxygenation (20% O_2). Parameters such as spike amplitude, spike slope, total active electrodes (TAE), and beats per minutes were assessed for hiPSC-CMs. For AC-16 CMs, RT-qPCR was used to determine mRNA expression levels of miR-24-3p and its targets, including *BIM*, and Western blotting used for determining the protein expression levels of BIM. To investigate the effects of miR-24-3p and hypoxia/reoxygenation on cell death, lactate dehydrogenase (LDH) and caspase-3 assays were performed in AC-16 CMs.

Results: TAE was reduced at the onset of hypoxia and at the onset of reoxygenation compared to baseline ($p<0.05$), while spike amplitude and spike slope were significantly reduced only during the latter ($p<0.001$). None of the parameters were significantly different from baseline at the end of the 4h reoxygenation period. MiR-24-3p did not have an effect on hiPSC-CM activity during hypoxia/reoxygenation. In AC-16 CMs, *BIM* mRNA expression was significantly upregulated during reoxygenation, compared to hypoxia ($p<0.01$) and normoxia ($p<0.001$). MiR-24-3p failed to suppress *BIM* mRNA expression levels in AC-16 CMs. The only significant difference seen in BIM protein expression levels was between the miR-24-3p mimic and inhibitor during hypoxia ($p<0.05$). Caspase-3 activity was elevated during hypoxia ($p<0.05$), but not reoxygenation. LDH activity increased during reoxygenation ($p<0.001$), however, data for the hypoxia condition from the LDH assay had to be excluded due to experimental errors. Therefore, it is not known whether LDH activity increased during hypoxia or not. Finally, caspase-3 and LDH activity was not influenced by miR-24-3p mimic nor inhibitor.

Conclusions: (1) Electrophysiological activity in hiPSC-CMs was reduced during hypoxia and worsened at the onset of reoxygenation. However, this was reversed with prolonged reoxygenation; (2) MiR-24-3p did not display significant cardioprotective effects in hiPSC-CMs exposed to hypoxia/reoxygenation, as there were no changes in functional output with neither the miR-24-3p mimic nor inhibitor; (3) In line with the data from hiPSC-CMs, miR-24-3p did not have a significant influence on AC-16 CMs.

Acknowledgements

The work presented in this thesis was carried out at the Department of Circulation and Medical Imaging, Faculty of Medicine and Health Sciences, Norwegian University of Science and Technology (NTNU) Trondheim. My supervisor for this work has been Associate Professor Morten Høydal and my co-supervisor has been Dr. Nathan Scrimgeour.

I want to express my gratitude to all the members of the Group of Molecular and Cellular Cardiology at NTNU for welcoming me to the team with open arms, and for providing support throughout the thesis project.

To Morten, thank you for having faith in me and for fostering my independence in the laboratory environment. Although it greatly enhanced my abilities to problem solve on my own, I knew your door was always open and that you were there to guide me if needed. It has been an honor to witness your positive nature and inclusiveness. To Nathan, thank you for having the answer to all the technical issues I encountered, for teaching me various techniques, and simply for being a pleasure to be around. To Gurdeep, I appreciate you being my side and contributing to my learning and the project with your valuable insights. If it were not for you, those countless hours in the laboratory would have been a lot less enjoyable.

Finally, I would like to offer my sincere gratitude to my fellow students, as well as the graduates, that I have gotten to know during the course of my studies at NTNU. It has been a delight to be a part of such a great working and social environment.

Table of Contents

List of Figures

List of Tables

1 Introduction

Ischemic heart disease (IHD) is the leading cause of global mortality, accounting for more than one in ten deaths worldwide each year. According to the World Health Organization (WHO) Global Health Estimates, deaths from IHD increased from 13.4% to 16.6 % in the time period from 2000-2016, with an estimated 9.4 million deaths in 2016 (1). Similarly, the global net burden, which additionally considers factors that negatively influence quality of life (e.g., years lived with disability and years of life lost), is expected to continue its rise, partly due to a growing and aging population (2). Recent decades have seen substantial improvements in treatment, preventative strategies, and management of risk factors (3). Yet, a substantial proportion of IHD-patients are likely to suffer from recurrent myocardial infarctions (MIs) and subsequent heart failure (HF) (4). MI is defined as myocardial cell death occurring along with an increase and/or a decrease of specific plasma biomarkers, particularly cardiac troponin (cTn), in the setting of myocardial ischemia (i.e. insufficient blood flow to the heart muscle) (5).

The infarct size is a central determinant of the long-term prognosis for patients that experience MI (6). Due to the minimal capacity of cardiomyocytes to regenerate, damage inflicted by MI is largely irreversible. Hence, limiting infarct size by restoring blood flow to the myocardium in a timely manner is critical (6). Currently, reperfusion is mainly achieved through the use of primary percutaneous intervention (PPCI) or thrombolytic agents (7; 8). The application of these therapies has been immensely successful in reducing acute and in-hospital mortality. However, it has subsequently led to increased morbidity and incidence of chronic HF, owing to improved survival of patients with severely depressed cardiac function both prior to and as a result of the MI (9). While effective in limiting ischemic damage, the reperfusion itself imposes acute stress that brings about pathological metabolic and biochemical events (10). This paradoxically provides an additional element of myocardial damage that can contribute up to 50% of the final infarct size, a phenomenon known as ischemia-reperfusion (I/R) injury (7; 11).

1.1 I/R injury and apoptotic cell death mechanisms

The mechanisms underlying the pathogenesis of I/R injury are not fully understood, and involves interplay between many factors integrated into a complex and dynamic network (10). It is initiated during ischemia and exacerbated by rapid reestablishment of blood supply during reperfusion. The main mediators of reperfusion-derived injury include intracellular Ca^{2+} overload, excessive reactive oxygen species (ROS) generation, inflammation, opening of the mitochondrial permeability transition pore (mPTP), and ion imbalance (7) (Figure 1). Moreover, I/R injury can be divided into four different types, each with distinct manifestations (7). Two types, including reperfusion-induced arrhythmias and myocardial stunning, are reversible. The former manifests as self-terminating ventricular arrhythmias and the latter causes temporary myocardial contractile dysfunction due to oxidative stress and Ca^{2+} overload (12; 13). The two remaining types are irreversible. One of them is described as reduced blood flow to the infarcted region despite successful opening of the culprit artery, called microvascular obstruction (14; 15),

while the other type is lethal reperfusion, which causes death of cardiomyocytes that were viable at the end of the ischemic event (16).

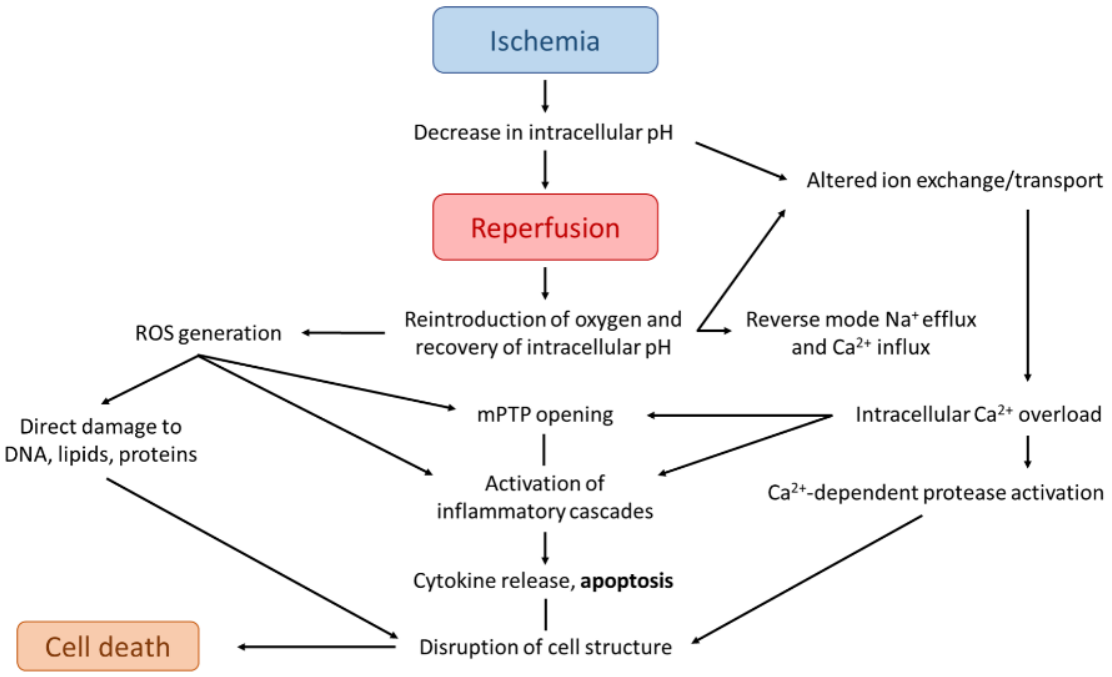

Figure 1. Major events contributing to ischemia/reperfusion injury. During ischemia, delivery of O_2 and nutrients to the cells is insufficient. This forces anaerobic metabolism to prevail, producing a drop in cellular pH (17). To counteract this, the Na^+/H^+ exchanger (NHE) ramps up excretion of H^+ while simultaneously creating a large influx of Na^+ (17). As a result, excess Na^+ leaves the cells through the Na^+/Ca^{2+} exchanger (NCX) and Ca^{2+} enters (18). The exchange and transport of ions are further disturbed by deactivation of ATPases due to depletion of cellular adenosine triphosphate (ATP). All these events contribute to intracellular and mitochondrial Ca^{2+} overload, which prompts a variety of cellularly lethal systems, for example by activating Ca^{2+} -dependent proteases, as well as triggering the opening of the mPTP during reperfusion (16; 19). Although reperfusion restores delivery of O_2 and substances required for aerobic ATP production, washing away of excess extracellular H^+ further increases proton gradient across the plasmalemma (20), thus intensifying reverse mode NHE activity and Ca^{2+} overload (10). Moreover, reintroduction of O_2 provokes a rise is the production of ROS, which is then able to modify biomolecules, resulting in inflammation, disruption of cellular structures, and cell death (21). Figure inspired by Sanada et al. (2011) (18) and Kalogeris et al. (2012) (10).

While most myocardial cell death in I/R injury happens by way of necrosis, others have been identified (reviewed in (22)). Consensus is yet to be reached in terms of the role apoptosis plays in I/R injury, and to what extent it impacts the ischemia and reperfusion phases (22). Still, apoptosis has been linked to a collection of assorted heart diseases (23). In contrast to necrosis, it is characterized by a highly programmed and genetically regulated caspase-dependent cell death that generally does not trigger an inflammatory response (24). While apoptosis is essential for development and maintenance of tissue homeostasis, inadequate or excessive activation can lead to disease pathogenesis.

There are two main pathways through which apoptosis can be propagated: the extrinsic and the intrinsic pathways. The extrinsic pathway is triggered in response to external stimuli, for example through the binding of ligands, such as tumor necrosis factor-α (TNF-α), Fas ligand (FasL), and TNF-related apoptosis inducing ligand (TRAIL), to their respective

death receptors located on the cell surface (25). The intrinsic pathway, in which the mitochondria are central contributors, is initiated by intracellular stress signals, e.g. DNA damage and hypoxia (26). In both pathways, the final outcome is activation of executioner caspases that cleave specific cellular substrates, resulting in apoptotic cell death (27). Connections between the pathways can also amplify signals and enhance the efficiency of killing.

1.2 miRNA function and biogenesis

Despite the efforts to elucidate molecular targets and pathways that contribute to I/R injury, translation of the accumulated understanding about the underlying mechanisms into a clinically valuable setting has been largely futile (28). It is only relatively recent that a class of small non-coding RNAs, microRNAs (miRNAs), were recognized as key players in the development and progression of cardiac diseases (29). These molecules, typically ~22 nucleotides (nts) in length, are involved in post-transcriptional regulation of messenger RNA (mRNA) expression, either by promoting degradation or inhibiting translation (30). This is achieved through the imperfect complementary binding of a miRNA to the 3' untranslated region (UTR), and in some cases the 5'-UTR, of its target mRNA (31; 32).

miRNAs influence most biological processes, with >60% of human protein-coding genes being estimated to be regulated by miRNAs (33). It has been shown that one miRNA can have up to hundreds of different mRNA targets, and that a single mRNA can be regulated by distinct miRNAs (32; 34). In addition, miRNAs can have synergistic effects, or the contrary, by which the activity of a given miRNA attenuates the activity of another (35). Canonical transcription of animal miRNA genes is carried out by RNA polymerase II (Pol II) (36), and is subject to regulation by Pol II-associated transcription factors and epigenetics (37). In the genome, miRNAs genes exist as either single genes or clusters containing up to several hundred different miRNAs (38) (Figure 2). MiRNAs genes are also commonly found embedded in introns of protein-coding genes (39).

The typical miRNA primary transcript (pri-miRNA) is a stem-loop structure with an imperfectly complementary paired stem and flanking segments (39). Pri-miRNAs are processed into precursor miRNAs (pre-miRNAs) through the excision of the flanking regions from the rest of the structure (40) (Figure 2). This is mediated by the microprocessor, a protein complex comprised primarily of Drosha and the double-stranded RNA (dsRNA)-binding protein (dsRBP) DiGeorge critical region 8 (DGCR8) (40; 41). After transportation out of the nucleus and to the cytosol, RNase III-type enzyme, Dicer, excises the loop from the stem of the pre-miRNA, thus creating a mature double-stranded miRNA ~22 nts in length (38). Finally, in a process termed RNA-induced silencing complex (RISC) loading, a member of the Argonaute (AGO) protein family discards one of the strands (passenger strand), while the remaining strand (guide strand) becomes the functional mature miRNA (42) (Figure 2).

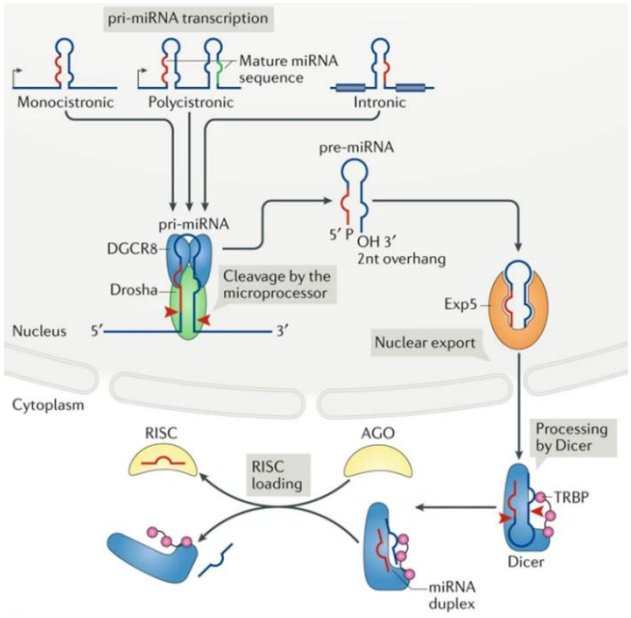

Figure 2. Overview of canonical animal miRNA biogenesis. miRNAs are encoded as individual genes (monocistronic), clusters (polycistronic), or in intronic regions of protein-coding genes (intronic) (43). These are transcribed by Pol II (not shown), creating pri-miRNAs that are cleaved by the microprocessor, a protein complex comprising DGCR8 and Drosha (40; 41). The resulting pre-miRNA is a stem-loop structure with 3' hydroxyl group (OH) overhangs of 2 nucleotides and a 5'phosphate (P) (43) . After being exported out of the nucleus and to the cytoplasm by Exportin 5 (Exp5), Dicer cleaves off the loop, generating a ds-miRNA duplex intermediate (38). One of the miRNA strands are then transferred to an AGO protein, forming RISC (42). This resulting miRNA strand is the mature miRNA (guide strand), while the other one (passenger strand) is discarded. Figure taken with permission from Treiber et al. (2018) (43).

In the heart, miRNAs take part in the regulation of growth, contractility, and cardiac rhythm (29). Dysregulated levels of miRNAs in the heart can thus have a profound effect on cardiac function, with specific miRNA expression levels found to be associated with certain pathological cardiac conditions (Figure 3). Cardiac-specific deletion of the miRNA-processing protein, Dicer, has been shown to cause cardiomyopathy and defects in mice leading to HF and neonatal death (44; 45). This demonstrates the importance of miRNAs in regulating the development and functioning of the heart. Due to the stability circulating of miRNAs in the plasma and the reliability in measuring these, the potential application of using them as biomarkers for cardiac disease has also attracted attention (46). For example, patients with HF display a signature increase and decrease in the levels of almost 30 different circulating miRNAs (47).

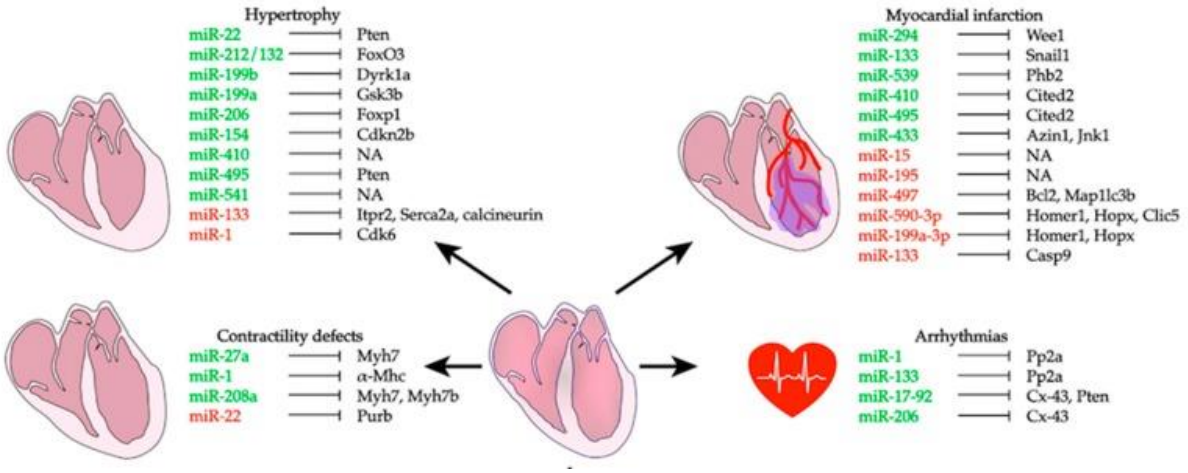

Figure 3. MiRNAs and respective targets commonly implicated in certain cardiac conditions. Green indicates upregulated and red indicates downregulated levels of miRNAs in the

different diseases. Adapted from Colpaert & Calore (2019) (29) under an open access Creative Commons CC BY 4.0 license.

1.3 miR-24 and BIM in myocardial hypoxia/reoxygenation and I/R

In unpublished left ventricular myocardial biopsy data collected by our research group (Group of Molecular and Cellular Cardiology, Norwegian University of Science and Technology) from patients with or without post-MI HF scheduled for coronary artery bypass graft surgery, a pattern of up- and downregulated miRNAs was found to be present in the patient group with post-MI HF. Included in the miRNAs that were significantly upregulated was miR-24-3p. Interestingly, one of the verified targets of miR-24-3p is the mRNA encoding the pro-apoptotic protein BCL-2-like protein 11 (BIM) (48; 49), a member of the B-cell lymphoma-2 (BCL-2) protein family (50). Considered gatekeepers of apoptosis, the members of this family have balancing and opposing effects, with BIM being a pro-apoptotic activator (50). In essence, BIM is able to stimulate pro-apoptotic effector proteins of the BCL-2 family, such as BCL2-antagonist (BAK) and BCL-2-associated X protein (BAX) (51). As described in Figure 4, BAK and BAX are important components of the intrinsic apoptotic pathway, by which activation of these proteins leads to mitochondrial release of cytochrome *c* (52).

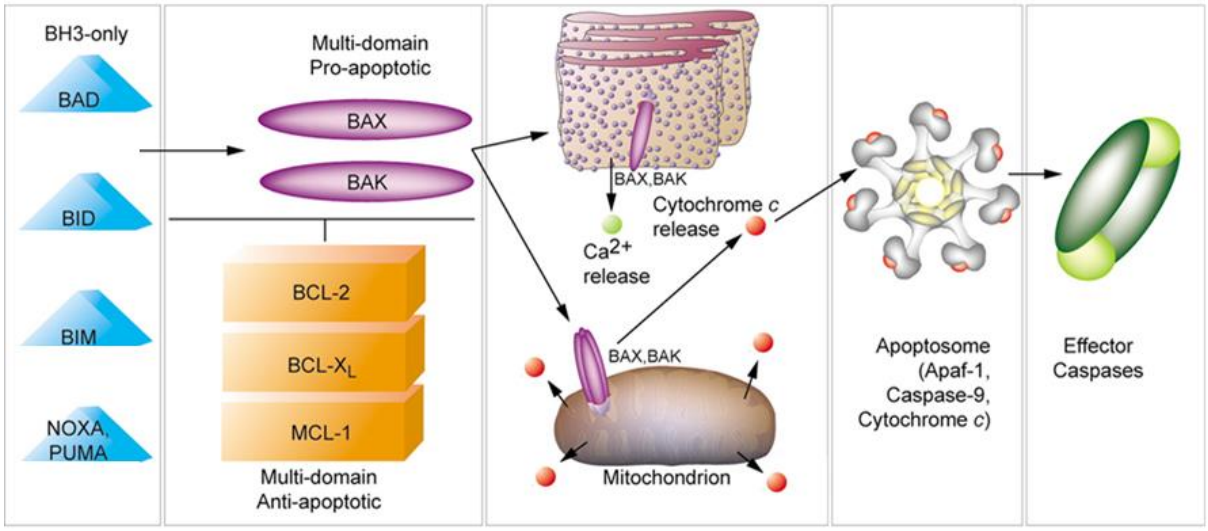

Figure 4. The BCL2-protein family can be divided into subclasses partly depending on the homology shared within four conserved regions, termed BCL-2 homology (BH) 1-4 domain (50; 52). BIM belongs to the BH3-only subfamily, of which members are pro-apoptotic activators. Following intracellular stress signals, the BH3-only proteins can activate multi-domain pro-apoptotic effectors, such as BAX and BAK (52). Upon activation, BAX and BAK undergo conformational change and insert into the endoplasmic/sarcoplasmic reticulum and mitochondrial outer membrane (MOM) as multimers to induce MOM permeabilization. Facilitated via the intrinsic pathway, this causes the release of pro-apoptotic mediators, such as cytochro*m*e c, from the intermembrane space into the cytosol (53). A caspase activation platform, the apoptosome, is then engaged to promote sequential activation of caspase-9 and the executioner caspases (-3 and -7), ultimately inducing the apoptotic phenotype (53). Adapted with permission Danial & Korsmeyer (2004) (52).

There has been differing reports for the expression of miR-24 after MI. Experiments conducted in both cell and animal models have demonstrated that miR-24-3p expression is decreased after hypoxia and acute MI (48; 49), while others have shown the opposite

(54). Experiments conducted in both cell and animal models have demonstrated that miR-24-3p expression is decreased after hypoxia and acute MI (48; 49), while others have shown the opposite (54). Common to these studies is that induction of miR-24-3p overexpression reduces apoptosis and markers of cellular damage, showing great promise for miR-24 mimics/agonists as potential therapeutics against apoptotic cell death in MI. However, it remains elusive from these findings alone whether the cardioprotective benefits of miR-24-3p come to effect during ischemia or reperfusion. Since treatment strategies for myocardial ischemia already have been successfully refined and established in the clinic, shedding light on the role of mir-24-3p during reperfusion may potentially be of more clinically significant value.

1.4 Modeling cardiac disease with hiPSC-CMs and MEA systems

Breakthrough discoveries by Yamanaka and colleagues showed that reprogramming of somatic cells into iPSCs (induced pluripotent stem cells) was possible through the use of only four transcription factors (OCT4/SOX2/c-MYC/KLF4) (55). Generated iPSCs can subsequently be differentiated into a variety of other somatic cells, such as cardiomyocytes (56) (Figure 5). The benefit of using iPSCs-derived cardiomyocytes (hiPSC-CMs) over immortalized cardiomyocytic cell lines for *in vitro* experiments is the closer recapitulation of native CMs (56). In contrast to immortalized CMs, hiPSC-CMs have not gone through genetic modification that allows them to be expanded indefinitely. Still, many somatic cells can be collected for reprogramming into iPSCs, thereby providing access to virtually unlimited amounts of iPSC-derived cells (57). However, maintaining cultures of iPSC is more technically challenging than immortalized cell lines (58). It requires a high degree of sterility and specialized trained personnel, which is not feasible for most standard laboratories (59). As such, many iPSC-derived cells have been made commercially available (58). While these commercially purchased cells are easier to handle, the number of cells that can be used for experiments is limited due to costs. An approach to manage this is to complement findings from iPSC-CMs with data from immortalized cell lines, as have been done in the present study. Here, we used AC-16 CMs, which is an immortalized cell line fused with primary adult ventricular CMs to assess changes at the protein and mRNA level (60). Although these do not recapitulate human cardiomyocyte function to the same extent as hiPSC-CMs, they are easy to genetically manipulate (e.g. through transfection with miRNA mimics/inhibitors) and yield high amounts of cellular material needed for various molecular assays.

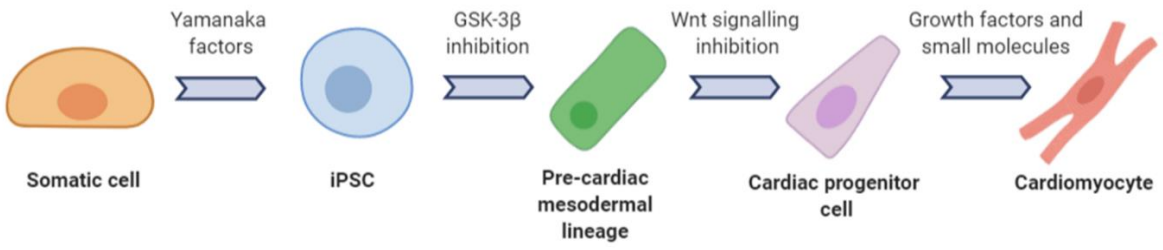

Figure 5. Schematic overview of stepwise generation of hiPSC-CMs. Somatic cells, for example dermal fibroblasts, can be differentiated into induced pluripotent stem cells (iPSCs) by delivery of Yamanaka transcription factors (OCT4/SOX2/c-MYC/KLF4) (54). These cells are then pushed towards the mesodermal lineage by GSK-3β inhibition (61), followed by canonical Wnt signalling inhibition to

produce cardiac progenitor cells (62). Functional cardiomyocytes can then be generated by treatment with a defined set of growth factors and small molecules.

Since hiPSC-CMs reflect the genetic profiles of the population from which they originated from, they open opportunities for personalized medicine and so-called "clinical trial in a dish'-concepts (56). Many of the drug candidates for cardiac indications that go through clinical trials never make it to the market. In 2018 alone, the US Food and Drug Administration approved 13 drugs for cancer, yet none for cardiac indications (63). Drug testing in hiPSC-CMs provides long-term cost benefits by ruling out ineffective and toxicity-inducing drugs at a pre-clinical stage (56). As such, many of the tedious, costly, and failed clinical trials for a potential drug candidate can be avoided. By reducing the need for animal testing, it has also attracted attention for the potential improvement of ethical issues regarding pre-clinical experiments conducted in animals. Although the applications of hiPSC-CMs are many (reviewed in (56)), so are the limitations. One of the major challenges is the lack of maturity of hiPSC-CMs, which resemble fetal CMs more than adult CMs in size, morphology, electrophysiology, response to calcium and beta-adrenergic stimuli, metabolism, and contractility (64; 65).

Emerging technologies able to capture field potentials of cells *in vitro* are paving the way for measuring electrophysiological activity of excitable cells (66). Multi-well microelectrode arrays (MEAs) provide a platform for measuring field potential (FP) and contractility of hiPSC-CMs in a high-throughput manner (66-68). They enable functional studies of hiPSC-CMs in disease modeling and pre-clinical testing of drug efficacy and toxicity. MEA systems allow for continuous real-time recordings, enhancing temporal resolution and making it possible to study changes over time (66). As ion imbalance is a major event in I/R injury (10) (Figure 1), MEA provides a unique platform for assessing electrophysiological changes governed by underlying ion currents through non-invasive recordings of extracellular FPs. The MEA system used in this study enables simultaneous measurements of a range of electrophysiological parameters (e.g., peak amplitudes, depolarization/repolarization, beat rate, FP duration, total active electrodes) in real-time (Axion BioSystems, Maestro Pro). This makes it a highly relevant choice for studying hypoxia-reoxygenation over a certain time-period. Specifically, we used this platform for measuring changes during an 18h hypoxia and 4h reoxygenation challenge in hiPSC-CMs transfected with either miR-24-3p-specific mimic or inhibitor. To my current knowledge, modeling of ischemia-reperfusion in hiPSC-CMs at this level of temporal resolution has not yet been explored.

2 Aims and hypotheses

To address the current challenges with I/R injury, the aims of this project were to:

1. Establish a model of hypoxia/reoxygenation (ischemia/reperfusion) in hiPSC-CMs, using a multi-well MEA system to capture and record electrical activity of these cells in real-time.
2. Explore the potential cardioprotective effects of miR-24-3p in hypoxia/reoxygenation by artificially up- and downregulating its expression in hiPSC-CMs using miR-24-3p mimics and inhibitors.
3. Verify the functional readouts from the hiPSC-CMs in AC-16 CMs by investigating changes at the mRNA and protein level, as well as cell death.

The hypotheses relating to these aims were:

1. Hypoxia impairs electrophysiological function in hiPSC-CMs, which is further exacerbated by reoxygenation.
2. MiR-24-3p provides cardioprotective benefits and ameliorates pathological disturbances caused by hypoxia/reoxygenation.
3. MiR-24-3p mimic reduces expression of its targets, including BIM, at both the mRNA and protein level. Cell death is attenuated with miR-24-3p mimics through targeting of BIM.

3 Methods

3.1 Cell culture

AC-16 cardiomyocytes (CMs) (Sigma-Aldrich, Darmstadt, Germany) and human induced pluripotent stem cell-derived cardiomyocytes (hiPSC-CMs) (Pluricyte) (Ncardia, Leiden, Netherlands) were used for all experiments. AC-16 CMs are immortalized cells derived from adult human ventricular cardiomyocytes and are proliferative *in vitro*. These cells were therefore used for methods requiring relatively large amount of cellular material, including Western blotting, RT-qPCR, LDH assay and caspase-3 assay (Figure 6). The hiPSC-CMs, or Pluricytes, display more mature phenotypes (e.g. electric and contractile activity) than AC-16 CMs, and are thus more ideal for assessing CM function. However, these cells were limited in number. For this reason, the Pluricytes were restricted to use for measuring electrophysiological parameters (Figure 6).

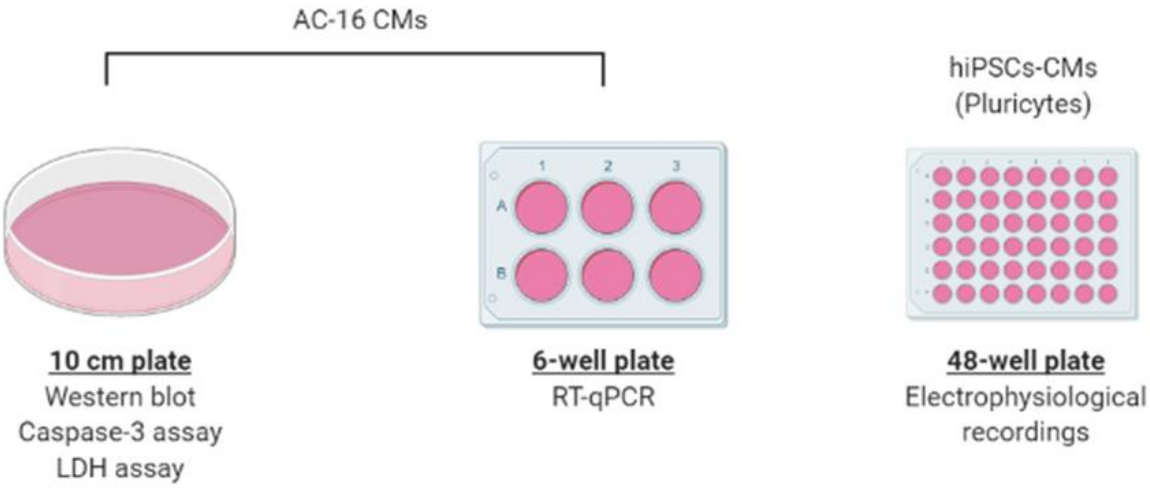

Figure 6. AC-16 CMs and hiPSC-CMs used for different analyses. AC-16 cardiomyocytes (CMs) used for western blot, caspase-3 assay, and LDH assay were seeded in 10 cm tissue culture plates. AC-16 CMs to be used for RNA extraction and subsequent RT-qPCR were seeded in 6-well plates. Human induced pluripotent stem cell-derived cardiomyocytes (hiPSC-CMs) (Pluricytes) used for electrophysiological recordings were seeded in 48-well plates.

3.1.1 AC-16 CMs

AC-16 CMs were grown and maintained in DMEM - F12 w/ L-Glutamine w/ 25 mM HEPES (Biowest, Nuaillé, France) supplemented with 12.5% Gibco™ fetal bovine serum (FBS) (Thermo Fisher Scientific, MA, USA) and 1% Antibiotic Antimycotic Solution (Sigma-Aldrich, Darmstadt, Germany). The cells, cultured in a humidified incubator with 5% CO_2 at 37°C, were split either 1:4, 1:5, or 1:8 every 4-5 days depending on confluency. This was done by aspirating the existing medium, followed by addition of trypsin and incubation at 37°C for 5-10 minutes before quenching with pre-warmed medium at a 1:3 ratio of trypsin:medium. The suspensions were then collected in 50mL tubes and spun down at

500 x *g* for 5 minutes at room temperature. Finally, the supernatants were discarded, and the cell pellets resuspended in fresh medium. The cells were seeded onto new 10 cm tissue culture plates (BioLite 100mm tissue culture dish, Thermo Fisher Scientific, MA, USA) for samples to be used in methods and assays requiring proteins, and in 6-well plates for samples to be used in protocols requiring RNA (Corning Costar 6-well plate, Saint-Louis, MO, US) (Figure 6). The AC-16 cells were used for up to 8 passages after initial thawing.

3.1.2 Pluricytes (hiPSC-CMs)

For electrophysiological recordings, the Pluricytes were used. These were thawed and plated onto Classic MEA 48-well plates (Axion BioSystems, Atlanta, GA, US) according to the cell supplier's instructions, including pre-coating and 3-hour incubation at 5% CO_2 at 37°C with fibronectin coating solution. Following aspiration of the fibronectin solution, thawed Pluricytes suspended in Pluricyte Cardiomyocyte Medium (PCM) (Ncardia, Leiden, Netherlands) were added. Both the fibronectin coating solution and cells were applied to the centre of the wells as 8µL droplets, covering the 16 inner electrodes while avoiding the four larger reference electrodes on the circumference of the wells (Figure 7). The seeded cells were maintained in 5% CO_2 at 37°C, with replacement of PCM (300µL/well) every other day until the hypoxia/reoxygenation experimental procedures (~8 days after seeding).

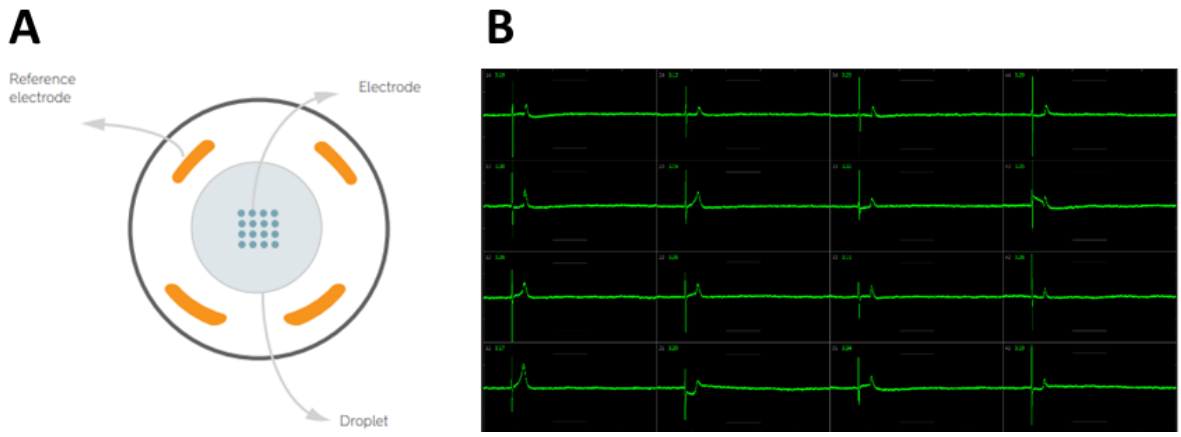

Figure 7. Seeding and functional output of hiPSC-CMs in a single well. (A) Illustration showing placement of the cell suspension droplet within a well, covering the 16 inner electrodes, while avoiding the four outer reference electrodes. (B) Representative picture of trace output from a single well of a 48-well plate, using the Axion Biosystems Maestro Pro system. Each square represents one of the 16 electrodes.

3.2 TargetScan

To explore other targets of miR-24-3p that may have a potential effect on the functional readings of the hiPSC-CMs, TargetScan (Release 7.2) was used to manually look for computationally verified targets that may be involved in electrophysiological changes (e.g. genes encoding subunits of ion channels).

3.3 Transfection

AC-16 cells and Pluricytes were transfected with miRIDIAN mir-24-3p mimic, inhibitor, or negative scramble (Horizon Discovery, UK). The scramble is a sequence from *Saccharomyces cerevisiae* with no known homology to any mammalian sequence and was used as negative control. Transfection was performed using Lipofectamine RNAiMAX diluted in Opti-MEM reduced serum medium according to the manufacturer's protocol (ThermoFisher Scientific, MA, USA), followed by incubation at 37°C for 3-4 hours. The medium was then aspirated and normal fresh medium without transfection reagent added. For 10 cm tissue culture plates, cells were transfected with 150 picomoles of mimic, inhibitor, or scramble RNA. Each well of the 6-well and 48-well plates were administered with 30 and 10 picomoles, respectively (Figure 8).

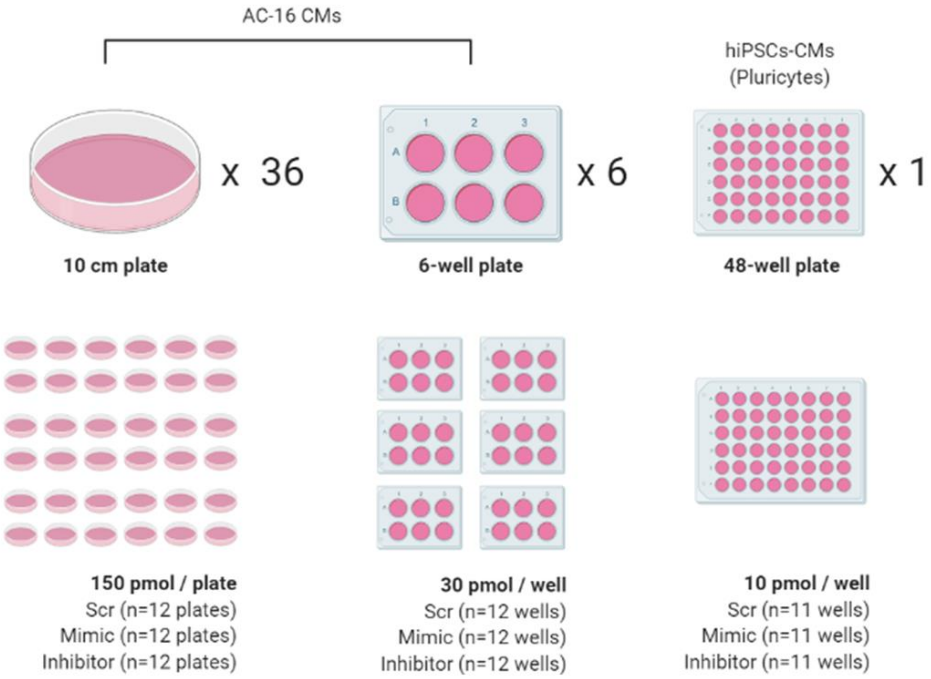

Figure 8. Transfection protocol. Cells were transfected with either scramble (Scr), mimic, or inhibitor. Each of the 10 cm tissue culture plates, wells in a 6-well plate, and wells in a 48-well plate were respectively transfected with 150 pmol, 30pmol, and 10pmol.

3.4 Hypoxia-reoxygenation experimental procedures

The AC-16 cells in 10 cm tissue culture plates and 6-well plates transfected with either mimic, inhibitor, or scramble (Figure 8) were equally allocated to each of the three environmental conditions (hypoxia, reoxygenation, and normoxia), giving rise to nine experimental groups and four biological replicates in each group (Figure 9). The whole 48-well plate containing hiPSC-CMs was subjected to all three conditions as the output from these cells were measured in real-time (Figure 9). Hypoxia was induced 42h after transfection by providing the cells with a hypoxia medium (93% DMEM, 5 mM creatine, 2.75 mM D–glucose solution, 2 mM glutamine, 10 mM HEPES, 2 mM L-carnitine, 1x non-essential amino acids, 1 mM sodium pyruvate, 5 mM taurine, 1x linoleic-oleic acid), followed by exposing them to hypoxic conditions (1% O_2 / 5% CO_2). Incubation in the

hypoxic and reoxygenation conditions was done in the Axion Maestro Pro incubator connected to a custom-built gas mixer for the hiPSC-CMs. For the AC-16 CMs, a specialized incubator (Galaxy 48R, New Brunswick, Birmingham, UK) was used to achieve hypoxic conditions.

For the reoxygenation group, there was an additional 4h incubation step in normal O_2 following the hypoxic challenge. Prior to placing the cells in normal O_2, medium was changed back from the hypoxia medium into the normal medium (Figure 9). The normoxic control group was exposed to the normal O_2 and medium throughout the entire experimental period (Figure 9). Cells were harvested by adding 1mL M-PER™ Mammalian Protein Extraction Reagent (ThermoFisher Scientific, MA, USA) containing 1% Halt™ Protease/Phosphotase Inhibitor Cocktail (ThermoFisher Scientific, MA, USA) in each plate for protein harvest and 300µL Qiazol from the miRNeasy Mini Kit (Qiagen, Hilden, Germany) in each well of the 6-well plate for RNA. The resulting protein and RNA lysate samples were scraped, collected, and stored at -20°C and -80°C, respectively. Harvests for LDH and caspase-3 assays were done differently and according to the manufacturers' instructions, described under "Cell death assays" below.

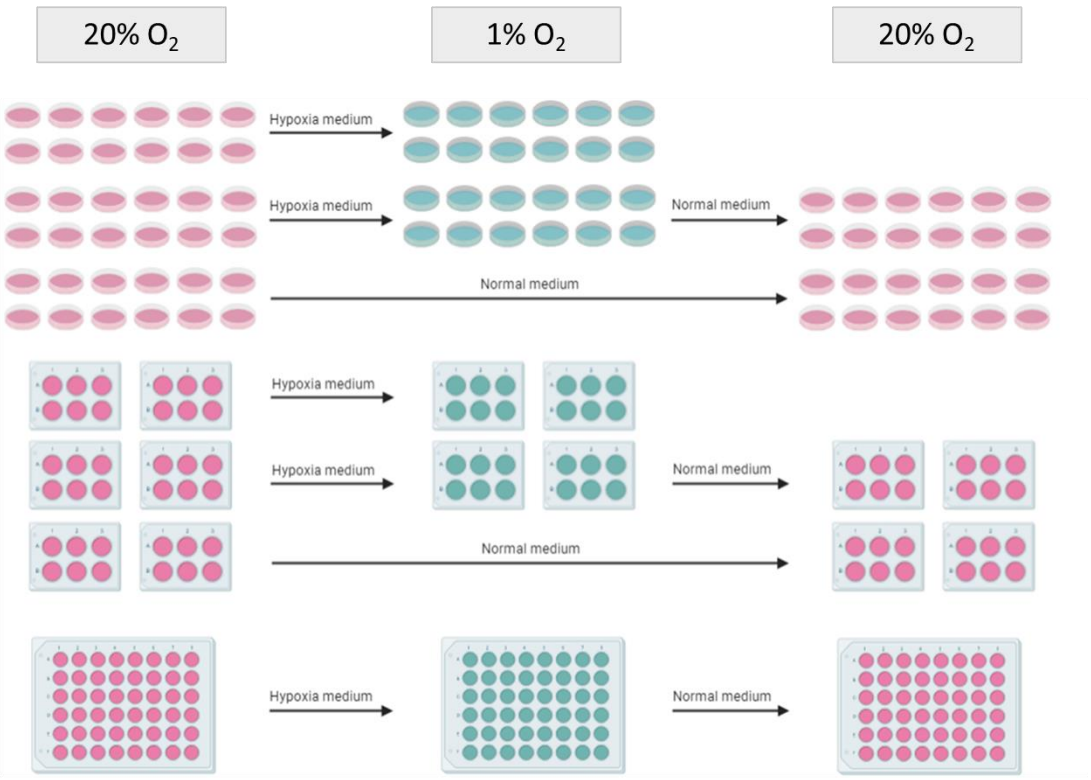

Figure 9. Hypoxia/reoxygenation protocol. Change into hypoxia medium (blue) was done for both the hypoxia group and reoxygenation group. The latter also had a change into normal medium (pink) before being placed back in 20% O_2. The normoxia group was maintained in normal medium (pink) and exposed to 20% O_2 throughout the experimental period. Each of the conditional groups had the following number of samples: n=12 plates and n=12 wells of 6-well plates. The entire 48-well plate containing hiPSC-CMs was exposed to all three conditions.

3.5 RNA isolation and determination of RNA expression levels by RT-qPCR

Total RNA from the cell lysates was extracted using the RNeasy Mini Kit (Spin technology protocol) as per instructions of the manufacturer (Qiagen, Hilden, Germany). The concentration and purity of the eluates were then measured using a Nanodrop 2000 UV-Vis spectrophotometer (ND-1000 3.2.1 software), followed by cDNA synthesis carried out according to the miScript II RT Kit protocol provided by the manufacturer (Qiagen, Hilden, Germany), using 1000ng RNA from each sample in the respective reaction mixes. Reverse transcription was performed using C1000 Thermocycler (Bio-Rad, Hercules, CA, US). After synthesis, the cDNA sample volumes were diluted 1:20 in H_2O.

For qPCR of protein-coding genes, primer pairs targeting *BCL2L11, KCNJ2, and SCN5a* and *RPL32*, were used, with the latter being the reference gene (Table 1). For validation of transfection with miR-24-3p mimic and inhibitor, miR-24-3p was amplified, with the small RNA molecule U6 small nuclear (RNU6-2) amplified as the reference gene. For both miR-24-3p and RNU 6-2, commercial universal primers from the miScript SYBR green PCR kit (Qiagen, Hilden, Germany) were used, as well as a miR-24-3p-specific primer with the sequence 5'-TGGCTCAGTTCAGCAGGAACAG-3' (mature miR-24-3p sequence from miRBase (69)) and an RNU 6-2-specific primer (miScript Primer Assays, Qiagen, Hilden, Germany). QuantiTect SYBR Green PCR Master Mix (Qiagen, Hilden, Germany), H_2O, and respective primers were mixed and prepared for each of the targets and transferred to a 96-well plate. Then, the diluted cDNA samples were transferred to the plate in triplicate, capped with strips and spun at 1000rpm for 1 min. The qPCR was performed using a CFX96 thermocycler with a C1000 real-time module (Bio-Rad, Hercules, CA, US). Following settings were used: 95 C for 15 min, (94°C for 15 s, 55°C for 30 s, 71°C for 30 s) x 42, 65°C -> 95°C with a 5°C increase every 5 s. Relative expression was determined by the $2-\Delta\Delta CT$ method (70). In brief, the $2^{-\Delta\Delta CT}$ method was calculated in a stepwise manner as such: 1) $\Delta CT = CT\ target - CT\ reference$; 2) $\Delta\Delta CT = \Delta CT\ (experiment\ group) - \Delta CT\ (control\ group)$; 3) $fold\ difference = 2^{-\Delta\Delta CT}$.

Table 1. List of primers targeting protein coding genes.

Target	Forward primer (5'-3')	Reverse primer (5'-3')	Source
BCL2L11	GATCGCATCATCGCGGTATT	CGCAGGCTGCAATTGTCTAC	Primer-BLAST (71)
KCNJ2	GTGCGAACCAACCGCTACA	CCAGCGAATGTCCACACAC	PrimerBank (72)
SCN5a	GGATCGAGACCATGTGGGAC	GTTCCGCTTTCCACTGCTG	Primer-BLAST (71)
RPL32	GCCCAAGATCGTCAAAAAGAGA	TCCGCCAGTTACGCTTAATTT	PrimerBank (72)

3.6 Protein concentration determination with Bradford assay

Protein concentration in the samples used in the LDH assay, caspase-3 assay, and western blot were determined by the Bradford assay. Standards were prepared through 1:2 serial dilutions of bovine serum albumin (BSA) in dH_2O. The amounts of BSA in the final reaction volume for each standard were 16µg, 8µg, 4µg, 2µg, 1µg, 0.5µg, 0.25µg, 0.125µg, 0.0625µg, and the standard blank at 0µg. The final reaction volume in each well was 200µL

for both the standards (160µL diluted BSA and 40µL Bradford reaction agent) and the samples (1µL sample supernatant, 159µL dH_2O and 40µL Bradford reaction agent). The absorbances were measured at a 595nm wavelength, using FLUOstar Omega microplate reader (BMG LABTECH, Offenburg, Germany). Finally, the absorbance values were used to plot the standard curve, in which the equation of the line was used to determine the protein concentration in the samples.

3.7 SDS-PAGE and Western blot

Polyacrylamide gels were hand casted, and consisted of a resolving part (12% acrylamide, 3.75 x 10^{-4} M Tris (pH 8.8), 0.1% SDS, 0.2% ammonium persulfate, 0.04% TEMED in ddH_2O) and a stacking part (5% acrylamide, 2.5 x 10^{-4} M Tris (pH 6.8), 0.1% SDS, 0.2% ammonium persulfate, 0.1% TEMED in ddH_2O) extending from the top to ~1cm below the wells. A 15-well comb was used to form the wells in the gel. A 1:5 ratio of Laemmli SDS Sample Buffer containing 15% 2-Mercaptoethanol (both from ThermoFisher Scientific, MA, USA) and protein lysates were then loaded into the wells. For optimization purposes, several rounds of SDS-PAGE/Western blots were run testing out different loading amounts of total protein, including ~20µg, ~40µg, ~55µg per well. Molecular weight markers used were a 1:1 mix of MagicMark XP Western Protein Standard (Invitrogen, Carlsbad, CA, USA) and Precision Plus Protein™ All Blue Prestained Protein Standard (Bio-Rad, Hercules, CA, USA), which were loaded into one of the edge wells of each gel. In tanks containing pre-prepared running buffer (25mM Tris, 190 mM glycine, 0.01% SDS in dH_2O) the gels were then run at 120V for 1.5 hours.

While the SDS-PAGE was running, Immuno-Blot PVDF membranes (Bio-Rad, Hercules, CA, US) were soaked in 100% methanol for ~2 minutes before being equilibrated in transfer buffer (25mM Tris and 190mM glycine in dH_2O, pH= 8.4), along with the cassettes, sponges, and transfer tissues that were to be used in the blotting step. After the SDS-PAGE, the gels were removed and placed in the equilibrated cassette system together with the membranes and ran at a constant current (0.2A for each of the tanks containing two cassettes) for ~1 hour and 20min. After, the blotted membranes were rinsed with TBST a few times prior to being blocked and incubated with 5% milk powder diluted in TBST for one hour and 15min at room temperature. The membranes were then rinsed at least three times each. For optimization purposes, two different anti-BIM primary antibodies were tested during separate rounds of Western blotting, using different dilutions. In the end, we chose to use the antibody at the dilution listed in Table 2. The membranes were incubated with primary antibody at 4°C with gentle rocking overnight. The day after, the membranes were rinsed 3 x 5min in TBST. Secondary antibody was added (Table 2), and the membranes incubated with gentle rocking at room temperature for 1h and 15min. Following incubation, the membranes were rinsed with TBST (6-8 x 5 min). SuperSignal™ West Pico PLUS Chemiluminescent Substrate was added as per the manufacturer's recommendations (ThermoFisher Scientific), before developing and imaging the membranes using Odyssey® Fc Imaging System (LI-COR Biosciences, Lincoln, NE, USA).

To re-probe the same membranes with beta-actin, the BIM-specific antibodies were stripped off using a stripping buffer (0.5M NaOH in ddH_2O) for ~10min. The same procedures starting from, and including, the 5% milk powder blocking step were then repeated, using β-Actin-specific antibodies (Table 2).

Table 2. List of antibodies (Abs) used in Western blotting.

1° Ab target	Host/isotope	Corresponding 2° Ab	1°/2° Ab dilution in TBST
BIM (Invitrogen, catalogue #: MA5-14848)	Rabbit/IgG	Goat anti Rabbit IgG (Bio-Rad, catalogue #: STAR124P)	1:1000/1:5000
β-Actin (Santa Cruz Biotechnology, catalogue #: sc-47778)	Mouse/IgG	Goat anti mouse IgG (Bio-Rad, catalogue #: STAR207P)	1:2500/1:5000

3.8 Cell death assays

Caspase-3 assay and LDH assay were performed on the same day, as the former required intracellular material (intracellular caspase-3), while the latter required material excreted in the media (extracellular LDH). As such, the material for both assays originated from the same sample plates. The caspase-3 colorimetric assay was performed as per the manufacturer's instructions (Caspase-3 Assay Kit (ab39401), Abcam, Cambridge, UK). Deviations included using the lysis buffer provided in the kit as a blank instead of the reaction buffer. The LDH assay was performed according to the instructions of the CytoTox 96® Non-Radioactive Cytotoxicity Assay (Promega, Madison, WI, US). As this assay had not been performed in our lab before, unexpected experimental errors occurred when following the instructions of the kit. This led to the hypoxic samples being too concentrated and out of the linear range required to detect reliable differences in the absorbances between the samples. Therefore, these data were excluded. Thus, for the normoxic and reoxygenation samples, which were collected at a later stage, a 1:10 dilutionof these samples using PBS was performed. Moreover, these occurrences lead to a 2h harvest delay of the samples of the samples exposed to reoxygenation and normoxia. As such the samples were exposed to 6h reoxygenation instead of 4h and 24h normoxia instead of 22h. This was the case for the samples used in both the LDH and caspase-3 assays. Caspase-3 sample absorbances were read at 405nm and LDH sample absorbances read at 495nm using FLUOstar Omega microplate reader (BMG LABTECH, Offenburg, Germany). These data were then normalized against the total protein concentration determined by the Bradford assay.

3.9 MEA recordings

Field potentials were recorded using standard cardiac settings (Axion Biosystems, Axis Navigator Software version 2.04) at baseline, post-transfection, hypoxia, and reoxygenation. Baseline was defined as pre-transfection, while two timepoints were recorded for post-transfection (18h and 42h) in normal O_2. Hypoxia (1% O_2) timepoints were recorded every hour for 19 hours, although only 18 hours were included in the analysis as this was our pre-determined endpoint. Reoxygenation (normal O_2) timepoints were subsequently recorded every hour for 4 hours. All recordings lasted for 5 minutes. The cells were allowed to equilibrate with the incubation chamber for at least 15 minutes before recording, whenever a new O_2 condition was introduced.

Output parameters included in the analysis were spike amplitude, total active electrodes, spike slope, and beat period (BPM). The latter was converted to beats per minute (60/beat

period). Raw data files were re-recorded using the AxIS digital filters. Standard settings were used, except for these detection thresholds: 150 µV, number of beats to analyze: 15 in the most stable region of the recording, 15-120BPM. Quiescent wells at baseline were excluded, resulting in n=11 wells per treatment group (scramble, miR-24-3p mimic, miR-24-3p inhibitor). Results were calculated in different ways:

1. To assess changes due to hypoxia/reoxygenation only (separately from miR-24-3p), results from the negative scramble group were calculated as percentage change from baseline.

2. To assess effects of miR-24-3p modulation and changes during normoxia post-transfection, results were calculated for all treatment groups as percentage change from baseline (pre-transfection).

3. To assess effects of miR-24-3p modulation during hypoxia/reoxygenation, results were calculated for all treatment groups as percentage change from the previous endpoint. This means that hypoxia was calculated as percentage change from 42h post-transfection and reoxygenation as percentage change from 18h hypoxia.

3.10 Statistical analysis

GraphPad Prism (GraphPad Software version 8.4.2, La Jolla CA, USA) was used for statistical analysis. Ordinary one-way ANOVA and mixed model ANOVA were performed for comparing three or more treatment groups, followed by Tukey's multiple comparisons test. The latter ANOVA was used only for analyzing the effect oxygen conditions in hiPSC-CMs, as all the wells in the plate were exposed to all conditions, thus a given well was matched across the conditions. An Unpaired student's t-test was performed for comparing two groups. All data are presented as mean ± SEM, and $p<0.5$ considered statistically significant.

4 Results

4.1 Effect of hypoxia/reoxygenation in hiPSC-CMs

Hypoxia was induced for 19h (only 18h taken into the analysis as this was our pre-determined endpoint) and reoxygenation for 4h. During this time, electrophysiological parameters, including total active electrodes (TAE), spike amplitude, spike slope, and beats per minutes (BPM) were recorded. To observe the effects of hypoxia/reoxygenation separately from treatment with miR-24-3p mimics and inhibitors, analysis was done for the negative scramble (Scr) group.

For most parameters, induction of hypoxia at 0h marked a decrease of general activity compared to baseline, though only significant for the TAE parameter ($p<0.05$) (Figure 10). An exception was spike amplitude, which was about the same as baseline at 0h hypoxia (6.6 ± 15.3%, p=NS). Only some of the timepoints during hypoxia were significantly different from induction of reoxygenation (0h) for TAE (hypoxia timepoints: 0-7h and 10-13h, $p<0.05$) and spike slope (hypoxia timepoints: 2h, 3h, and 5h, $p<0.05$), while no such difference was seen for any of the hypoxia timepoints of the spike amplitude and BPM parameters (Figure 10). There was a significant change with induction of reoxygenation in all parameters, except BPM. Reoxygenation produced an initial fall compared to baseline (TAE: -62.8 ± 10%, $p<0.05$; spike amplitude: -77.3 ± 5%, $p<0.001$; spike slope: -88.7 ± 6%, $p<0.001$), which eventually climbed up to the similar levels as those during hypoxia (Figure 10).

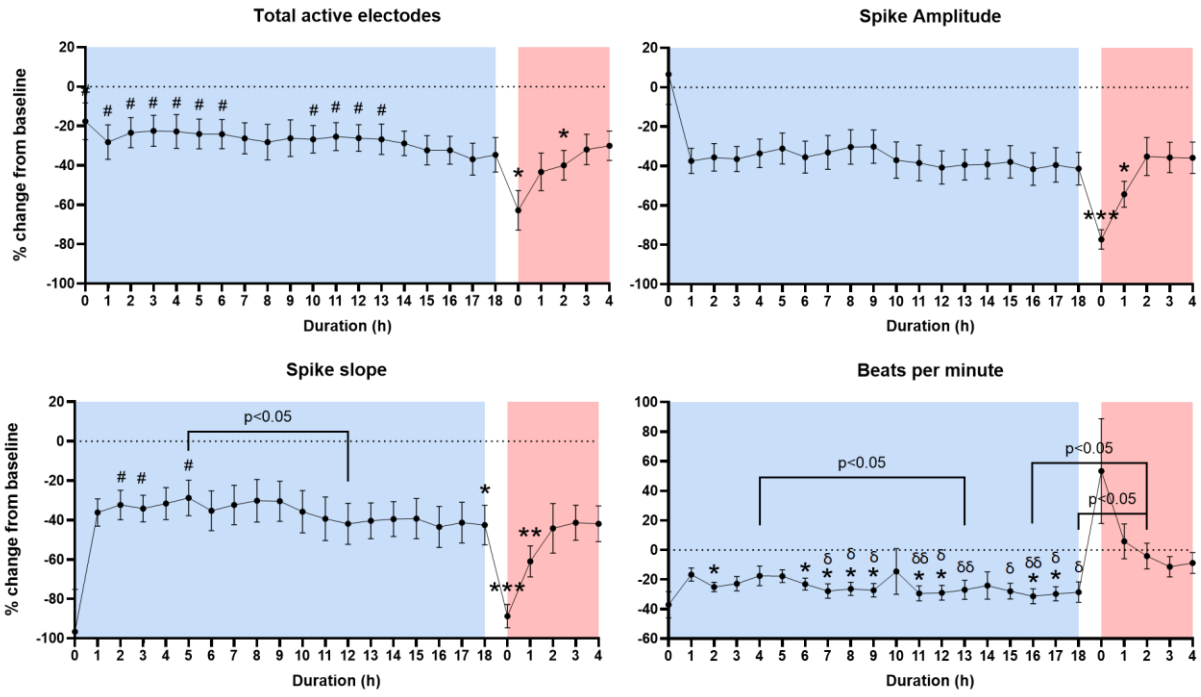

Figure 10. Effect of hypoxia/reoxygenation in the hiPSC-CM scramble group. Effect of 18h hypoxia (1% O_2) (blue) and 4h reoxygenation(20% O_2) (red) on total active electrodes (out of 16), spike amplitude, spike slope, beats per minute of the hiPSC-CMs transfected with negative scramble. Baseline is shown as the stippled line. *p<0.05, **p<0.01, ***p<0.001 versus baseline; #p<0.05 versus initiation of reoxygenation (0h); δp<0.05, δδp<0.01 versus 2h reoxygenation.

Representative recordings of heat plots from Axis Navigator Software (version 2.04) show electrical activity of hiPSC-CMs at the different endpoints (Figure 11). The type and the intensity of the colours depict the extent of activity, measured in spike amplitude. For example, seven of the eight wells in the bottom row are black, as there were no cells seeded in those wells, while the leftmost well in the same row show all 16 electrodes picking up electrical activity during baseline and 42h post-transfection (Figure 11A and 11B). The entire plots for baseline (Figure 11A) and 42h-post transfection (Figure 11B) are also notably different from the hypoxia plot (Figure 11C), where there is visually less activity, which picks up again slightly in the reoxygenation plot (Figure 11D). This corresponds to the data collected for the total active electrodes and spike amplitude parameters: the hypoxia endpoint is slightly lower than the reoxygenation endpoint, with both endpoints being less than baseline and 42h post-transfection (Figure 10).

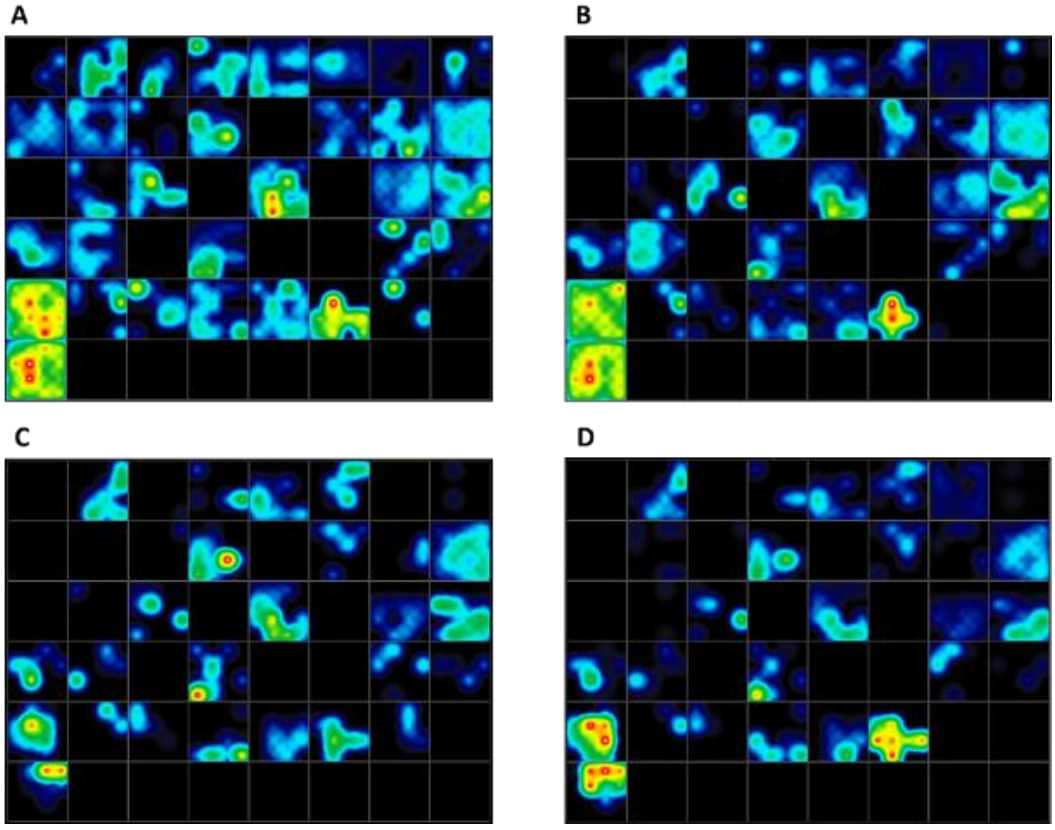

Figure 11. Representative heat plots of depolarization peak amplitudes. Heat plots during (A) baseline; (B) post-transfection (42h); (C) end of hypoxia; (D) end of reoxygenation. Each square in a plot represents one of the 48 wells in the plate. The 16 electrodes in each well detecting field potential are in different colours, depending on extent of amplitude. Output from AxiS Navigator Software (Axion Biosystems, version 2.04).

4.2 Effect of miR-24-3p in hiPSC-CMs during normoxia and hypoxia/reoxygenation

From the TargetScan analysis, *SCN5a* and *KCNJ2* were identified as being targets of miR-24-3p directly (not shown). These encode subunits of the cardiac sodium channel, $Na_V1.5$, and inward rectifier potassium channel, $K_{ir}2.1$, respectively. Since these play a role in electrophysiological function of cardiomyocytes, it was expected that miR-24-3p mimic and inhibitor would have an effect on the functional readings. Moreover, miR-24-3p targets *BIM*, thus it was hypothesised that miR-24-3p mimic would have a protective effect on the cells, which could have been seen for example in the TAE parameter. However, transfection with mir-24-3p mimic and inhibitor had no statistically significant effect on electrophysiological responses in normoxia (Figure 12) nor hypoxia/reoxygenation (Figure 13).

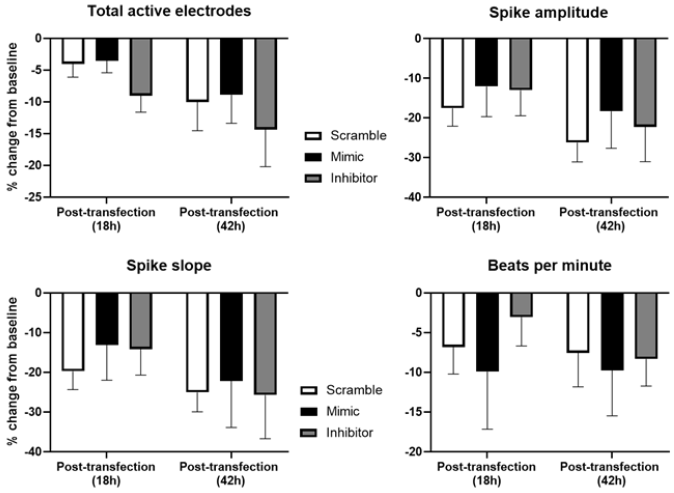

Figure 12. Effect of miR-24-3p mimic and inhibitor in hiPSC-CMs during normoxia. Two timepoints were recorded after transfection under normal O_2 conditions (20%) (18h post-transfection and 42h post-transfection). Parameters analysed were total active electrodes, spike amplitude, spike slope, beats per minute.

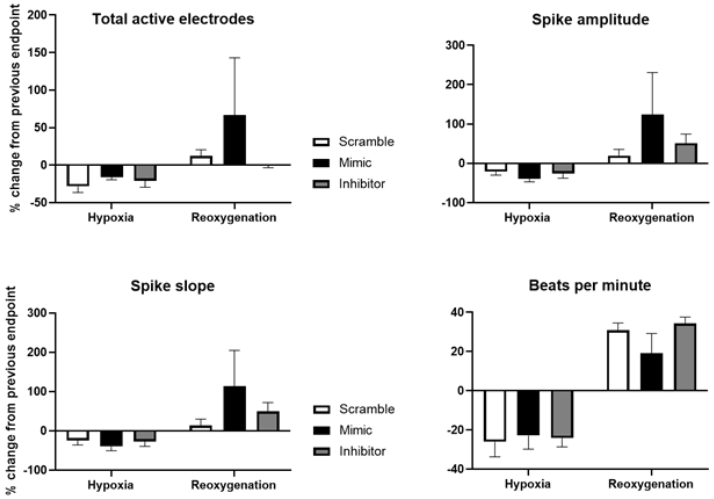

Figure 13. Effect of miR-24-3p mimic and inhibitor in hiPSC-CMs during hypoxia/reoxygenation. Parameters analyzed were total active electrodes, spike amplitude, spike slope, beats per minute at the end of hypoxia (18h 1% O_2) and reoxygenation (18h 1% O_2 and 4h 20% O_2).

4.3 RT-qPCR analysis of miR-24-3p and its targets in AC-16 CMs

To investigate the effect of the O_2 conditions on *BIM* mRNA expression levels alone, analysis of only the scramble treated – AC-16 CMs in the different conditions was conducted. This showed that *BIM* levels were increased in the reoxygenation condition when compared to both normoxia (1.5-fold, $p<0.001$) and hypoxia (1.4-fold, $p<0.01$) (Figure 14A). No such difference was found between the hypoxic and normoxic conditions.

AC-16 cells transfected with mir-24-3p mimics showed a significantly higher expression of miR-24-3p compared to both mir-24-3p inhibitor and negative scramble, in all respective conditions (Figure 14B). Expression levels of mir-24-3p were 5.5-fold ($p<0.001$), 7-fold ($p<0.01$), and 3.5-fold ($p<0.05$) that of scramble in normoxic, hypoxic, and reoxygenated conditions, respectively (Figure 14B). On the other hand, transfection with miR-24-3p inhibitor showed a trend towards lower expression compared to scramble (-3.7-fold [normoxia], -3.4-fold [hypoxia], -4.6-fold [reoxygenation]), although not statistically significant (Figure 14B). The miR-24-3p expression levels did not change in the scramble group between the conditions, indicating that miR-24-3p is not upregulated in these cells in response to hypoxia/reoxygenation (Figure 14B).

Transfection with mir-24-3p mimic and inhibitor did not influence the mRNA expression levels of *BIM*, which showed no statistically significant difference in expression levels between any of the treatment groups in any of the conditions (Figure 14C). Amplification of *SCN5a* and *KCNJ2* were unsuccessful, i.e. Ct values >38 (not shown).

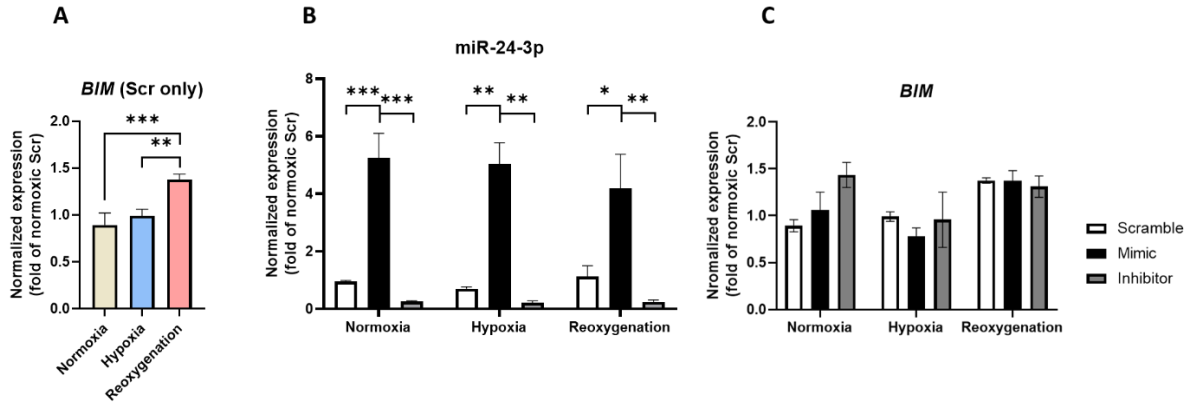

Figure 14. mRNA expression levels of miR-24-3p and *BIM* in AC-16 CMs. Normalized mRNA expression level at the end of normoxia (22h 20% O_2), hypoxia (18h 1% O_2), and reoxygenation (18h 1% O_2 and 4h 20% O_2) of (A) *BIM* in the negative scramble groups (B) miR-24-3p in all treatment groups (C) *BIM* in all treatment groups *p<0.05, **p<0.01, ***p<0.001.

4.4 Western blot analysis of BIM in AC-16 CMs

As with mRNA expression (Figure 14A), BIM protein expression was elevated with reoxygenation compared to normoxia, when comparing the negative scramble groups in each condition (2.5-fold, $p<0.05$) (Figure 15A). Moreover, there was no significant difference in BIM levels between reoxygenation and hypoxia. However, in contrast to mRNA

expression levels, there was no significant difference in BIM levels between reoxygenation and hypoxia.

The western blots revealed a trend of decreased and increased protein expression of BIM in AC-CMs transfected with miR-24-3p mimic and inhibitor, respectively, although only a statistical significant difference was found during hypoxia, between the mimic and inhibitor groups (1.9-fold, $p<0.05$) (Figure 15B and 15C).

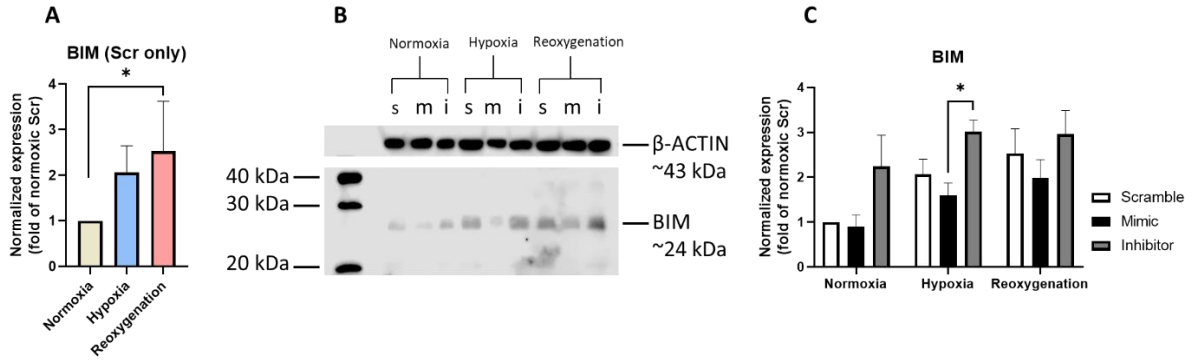

Figure 15. Protein expression levels of BIM in AC-16 CMs. (A) Normalized protein expression level of BIM at the end of normoxia (22h 20% O_2), hypoxia (18h 1% O_2), and reoxygenation (18h 1% O_2 and 4h 20% O_2) in the negative scramble groups. (B) Representative Western blot picture. Scramble, mimic, and inhibitor are denoted as s, m, and I, respectively. (C) Normalized protein expression level of BIM at the end of normoxia (22h 20% O_2), hypoxia (18h 1% O_2), and reoxygenation (18h 1% O_2 and 4h 20% O_2) in all treatment groups. *$p<0.05$.

4.5 Cell death analysis in AC-16 CMs

Hypoxia (18h) induced caspase-3 activity compared to normoxia (24h) in the scramble groups of the respective conditions (1.6-fold, $p<0.05$) (Figure 16A). The same effect was not imposed by reoxygenation. LDH activity was markedly enhanced by 6h reoxygenation compared to 24h normoxia, when comparing the two scramble-treated groups (5.1-fold, $p<0.001$) (Figure 16B). Neither mir-24-3p mimic nor inhibitor influenced caspase-3 activity (Figure 16C), which was also the case for LDH activity (Figure 16D). As mentioned in methods, due to experimental errors that occurred with the LDH assay for the hypoxic samples, these data were excluded. Therefore, only comparisons between reoxygenation and normoxia was done.

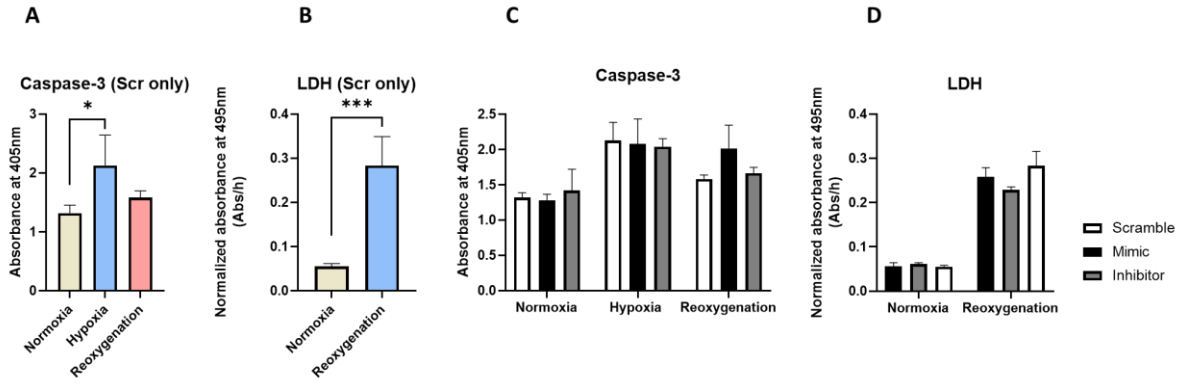

Figure 16. LDH and Caspase-3 activity. (A) Caspase-3 activity at the end of normoxia (24h 20% O_2), hypoxia (18h 1% O_2), and reoxygenation (24h 1% O_2 and 6h 20% O_2) in the negative scramble groups. (B) LDH activity at the end of normoxia (24h 20% O_2) and reoxygenation (24h 1% O_2 and 6h 20% O_2) in the negative scramble groups. (C) Caspase-3 activity at the end of normoxia (24h 20% O_2), hypoxia (18h 1% O_2), and reoxygenation (24h 1% O_2 and 6h 20% O_2) in all treatment groups. (D) LDH activity at the end of normoxia (24h 20% O_2) and reoxygenation (24h 1% O_2 and 6h 20% O_2) in all treatment groups. *$p<0.05$, ***$p<0.01$.

5 Discussion

In the present study, recordings of electrophysiological parameters were performed on hiPSC-CMs to determine functional responses to hypoxia/reoxygenation and modulation by miR-24-3p-specific mimics and inhibitors. The functional outputs read from the hiPSC-CMs were then supported by data from various molecular assays in AC-16 CMs. The main findings demonstrate temporally dynamic electrophysiological changes in hiPS-CMs during hypoxia/reoxygenation. Most notable was the overall reduction in electrophysiological parameters at the onset of reoxygenation. However, no significant change was observed at the end of the hypoxia/reoxygenation challenge compared to baseline, indicating a recovery of electrophysiological activity with persistent reoxygenation. In terms of cardioprotective effects by miR-24-3p, we show that miR-24-3p did not have an influence on functional activity during normoxia nor hypoxia/reoxygenation. The findings from the hiPSC-CMs were validated in AC-16 CMs, in which hypoxia and reoxygenation produced changes in *BIM* mRNA and BIM protein expression levels, as well as cell death. Furthermore, miR-24-3p did not affect mRNA expression levels of *BIM* nor cell death. There was a difference in BIM protein expression between miR-24-3p mimic and inhibitor, although only in hypoxia.

In hiPSC-CMs, reoxygenation produced a significant initial decrease compared to baseline for all parameters analyzed, except for beats per minute (BPM). This indicates that reoxygenation indeed amplifies the effects of hypoxia, at least for measurements from extracellular field potentials (FPs). FP measurements of BPM and spike amplitude are considered to resemble heart rate and QRS amplitude, respectively, in an electrocardiogram (ECG) (73). Although the gold standard for measuring action potentials (APs) in cardiomyocytes is through manual patch-clamping methods, these are often labor intensive and technically challenging, low-throughput at the single-cell level, and requires relatively good biophysics knowledge for data interpretation (66). In comparison, MEA systems are more automated, easier to use, and higher throughput. Since patch clamping techniques measure APs, they provide more accurate measurements of the ion fluctuations across the cell membrane than extracellular FP measurements. However, it has recently been shown that FPs can directly be translated to the underlying APs in a reliable fashion (74). In that report it was demonstrated that MEA-based assessment generated electrophysiological data that accurately corresponded to AP data acquired with patch clamping techniques in human embryonic stem CMs and primary mouse CMs. Thus, the data acquired from the MEA system and hiPSC-CMs used in the present study may provide valuable insight into the temporal changes that occur in CMs during I/R injury.

The electrophysiological changes in hiPSC-CMs occurring at the initial phase of reoxygenation were fully reversed to the levels observed during hypoxia, as the duration of reoxygenation persisted. These data suggest that the changes caused non-permanent damage to the cells, and that prolonged reoxygenation eventually salvaged the damage inflicted by sudden reintroduction of O_2 and change of medium. The sudden change in the parametric output at the onset of reoxygenation might be explained by worsening of ion imbalances during hypoxia, such as increased Na^+ and Ca^{2+} in the cell and K^+ outside the cell (75). Since reoxygenation recovers ATP synthesis, the ATP-dependent channels that take up free Ca^{2+} into the sarcoplasmic reticulum (SR) are reactivated, leading to Ca^{2+}-induced Ca^{2+} release (CICR) from the SR (76). Moreover, since medium change removes the H^+ accumulated in the media during hypoxia, there will be a higher proton gradient across the cell membrane. This may lead to enhanced activation of the NHE, and as a consequence, further Ca^{2+} loading through the NCX working in reverse (76).

It has been shown that during acute phases of reperfusion/reoxygenation, the SR is overwhelmed by Ca^{2+}, causing repeated CICR cycles that produce oscillations in Ca^{2+} levels, and thereby fluctuations in membrane potential (77). These oscillations have been

proposed to be a cause of reperfusion-induced arrhythmias, caused by delayed afterdepolarizations (78). Moreover, Ca^{2+} oscillations can cause excessive contractile activity, which can lead to hypercontracture (79-82). In our findings, BPM increased at the onset of reoxygenation, although insignificant. Despite BPM being increased, it does not mean that the actual strength of the beat/contraction was increased. This is for example demonstrated by the simultaneous decrease in the spike amplitude parameter. Since the parametric levels were brought back to those of hypoxia at the end of reoxygenation, it is thus likely that the damage inflicted was related to the reversible types of reperfusion injury that are observed *in vivo*, namely reperfusion-arrhythmia and myocardial stunning.

It is interesting that caspase-3 activity in the data from the AC-16 CMs showed a significant increase during hypoxia compared to normoxia, but that no change was seen after reoxygenation. In line with the hiPSC-CM data, end of reoxygenation was not significantly different from normoxia nor hypoxia. At the initiation of reoxygenation, increased CICR also triggers Ca^{2+} uptake into mitochondria via the Ca^{2+} uniporter, which have been shown to cause opening of the mitochondrial permeability transition pore (mPTP) and release of cytochrome *c* (83). Although the latter activates apoptosis, it could be that prolonged reoxygenation dilutes this effect if Ca^{2+} levels are brought back to normal after reoxygenation. Since the reoxygenation duration for the cell death assay samples was prolonged to 6h due to technical difficulties with the experiments, it could be that by the time of cell harvest and reading of absorbances, caspase-3 levels or activity were significantly decreased. In fact, it has been shown that the active form of caspase-3 exhibits a half-life of 8h (84). Hence, if cytochrome *c* release caused by mitochondrial Ca^{2+} overload occurs during the acute phase of reoxygenation, a marked increase in caspase-3 activity would not be observed at a later phase, as was seen in our data.

MiR-24-3p mimic and inhibitor did not elicit a significant response in the hiPSC-CMs. Functional activity of the hiPSC-CMs remained unchanged during both normoxia and hypoxia. These findings were unexpected as miR-24-3p targets genes encoding components of ion channels important for cardiac electrophysiological function, such as *SCN5a* and *KCNJ2.* These genes have been found to be modulated by miR-24-3p in previous studies (85; 86), which was in line with our findings from the TargetScan analysis. The *SCN5a* gene encodes the pore-forming α-subunit of the cardiac Na^+ channel, $Na_v1.5$ (87). This channel is responsible for the rapid influx of Na^+ during the AP upstroke, as well as for the late sodium current (87). In theory, inhibition with miR-24-3p mimic would cause less activity of this channel. Drug-induced block of the Na^+ inward current via the Nav1.5 is for example associated with a prolonged QRS on the ECG (88). Therefore, in the present study, it was expected that there would be a decrease in the spike slope and spike amplitude parameters with the miR-24-3p mimic. Since amplification of these transcripts in AC-16 CMs using RT-qPCR failed, mRNA levels could not be assessed. Due to limited time, it was not feasible to re-design primers for optimization of PCR-amplification of these targets. Therefore, it was subsequently decided that Western blotting would not be performed for the protein products of these genes. Nonetheless, for the scope of this project, unchanged functional outputs from the hiPSC-CMs with the miR-24-3p mimic and inhibitor did not warrant further exploration of these targets.

In AC-16 CMs, miR-24-3p mimics and inhibitors were found to be successfully introduced into the cells. Corresponding suppression of *BIM* by miR-24-3p mimics was not seen at the transcriptional level. As such, it is not certain that the presence of miR-24-3p mimic and inhibitor was sufficient to down- and upregulate *BIM* expression, respectively. A different explanation for our conflicting results is that miRNAs do not function as naked RNAs. Instead, they function in the form of ribonucleoprotein complexes, miRISCs (miRNA-induced silencing complexes) (89). The most prominent protein components of miRISC are Argonaute (AGO) and GW182 [glycine-tryptophan (GW) repeat-containing protein of 182 kDa] family proteins (89). The RT-qPCR method used for validating transfection of miRNAs is limited in the sense that it detects the presence of the mimic, but not whether it is in its incorporated into miRISC. Therefore, confirming the presence of miR-24-3p alone did not provide information about whether translational repression of *BIM* was achieved. For these

purposes, alternative methods for validating miRNA-mediated regulation, such as luciferase reporter gene assays, can be used (90). This could be valuable for future studies, however, in the present study, we decided to complement the mRNA data with output from the protein level, where the potential effects of miR-24-3p arguably exert the final and most important functions.

It has not been established whether miR-24-3p suppresses *BIM* through inhibiting translation or degradation/destabilization of the *BIM* mRNA transcript. Of the AGO1-4 proteins, only AGO2 possesses the ability to cleave and degrade mRNA targets (91). This is achieved when there is a perfect Watson and Crick pairing of the miRNA seed sequence (2-7 nt position from the 5' end) and the miRNA regulatory element (MRE) of the mRNA target (35). In mammals, imperfect pairing and inhibition of translation is more common than cleavage (91). The former mechanism could explain how BIM protein expression, in our findings, is significantly reduced with the miR-24-3p mimic in hypoxia, whereas *BIM* mRNA expression is not. Previous reports have suggested that mechanisms of translational repression occur through decreased initiation of translation (92; 93), as well as through ribosome drop-off (94). On the other hand, others have suggested that decreased protein production is primarily attributable to lowered mRNA levels (95; 96).

The kinetics of miRNA regulation has also been explored, showing that inhibition of translation occurs during the initial stages, followed by destabilization and decay as a result of deadenylation of the Poly(A) tail at a later stage (97; 98). Unchanged mRNA levels of *BIM* could thus be a "snapshot" of the former. In that case, the time of cell harvest and the rapidness of transcript decay after destabilization would be of major influence. While our data only show a statistically significant reduction of BIM protein level with the miR-24-3p mimic in hypoxia group, the trend towards reduced BIM protein expression with the mimic and increased expression with the inhibitor in all conditions is noteworthy. Given that an inverse relationship between miR-24-3p levels and *BIM* mRNA levels was not observed, further optimization of the Western blot procedures would be interesting to resolve whether BIM protein levels indeed were decreased with the mimic during hypoxia.

Decade-old studies showed that direct inhibition of caspase-3 attenuates apoptosis during I/R (99-101). In this current study, it was hypothesized that inhibition of BIM by miR-24-3p would decrease caspase-3 mediated apoptosis. However, previous reports have demonstrated that miR-24-3p increases apoptosis in cardiomyocyte (CM) and non-CM cardiac cells after hypoxia/reoxygenation and I/R (102). Cells from mice after MI show that miR-24-3p levels were significantly upregulated in cardiac endothelial cells, but not in CMs (102). The endothelial cells with upregulated miR-24-3p levels showed increased apoptosis, while miR-24-3p antagonism successfully attenuated apoptosis (102). Parts of these findings were confirmed by our data from AC-16 CMs, in that no change in miR-24-3p levels was observed between the scramble groups exposed to normoxia, hypoxia, and reoxygenation. However, cell death assays showed no difference between treatment with negative scramble, miR-24-3p mimic, and inhibitor. If BIM was not effectively reduced by miR-24-3p, then anti-apoptotic effects through targeting of BIM would not be present and thus not influence cell death. Other reports have supported our original hypothesis, and observed that miR-24-3p mimic ameliorates apoptosis during MI (48). Given the conflicting results, additional and repeated rounds of experiments need to be performed in order to draw conclusions relating to our hypothesis.

5.1 LIMITATIONS

One of the major limitations of modelling hypoxia/reoxygenation (ischemia/reperfusion) in hiPSC-CMs is the lack of maturity. Therefore, careful consideration needs to be taken when drawing conclusions from hypoxia/reoxygenation experiments using hiPSC-CMs. Moreover, since AC-16 CMs do not recapitulate the physiology of native CMs to the same extent as hiPSC-CMs, findings from AC-16 CMs cells cannot conclusively be compared to those of hiPSC-CMs. In this study, data collected from AC-16 CMs were mainly to support the

functional outputs from the hiPSC-CMs. Conversely, changes in electrophysiological activity of hiPSC-CMs may not produce observable changes in AC-16 CMs. As such, these cell types are best used in conjunction for verification purposes.

Another major limitation of this study was the lack of biological replicates. Insufficient time made it non-feasible to repeat the different methods once optimized. Moreover, some methods were not fully optimized (e.g. Western blotting, PCR-amplification of *SCN5a* and *KCJN2,* cell death assays). To account for inter-experimental variation, multiple repeats of the same experiment would have to be performed. This would also increase statistical power and produce more robust and reliable data. Also, other methods could also have been applied, for example luciferase gene reporter assay to validate that the miR-24-3p mimic we transfected with was functional. Furthermore, Western blotting is semi-quantitative and is not a precise method for protein quantification. Taken together, this thesis project can be viewed as a basis for future work.

6 Conclusions

This project represents a first attempt to model ischemia/reperfusion in hiPSC-CMs in real-time, using a multi-well microelectrode array system. Although further studies need to be conducted and much remains to be improved, it has provided a unique insight into the temporal electrophysiological changes that occur in CMs during ischemia/reperfusion. With further studies, this could potentially help identify at which time during reperfusion that a cardioprotective therapeutic can exert the maximum benefit. Relating to our initial aims and hypotheses, the conclusions are:

1. Electrophysiological activity measured in hiPSC-CMs was reduced during hypoxia and worsened at the onset of reoxygenation. This worsening was fully reversed by the end of the reoxygenation period of four hours, indicating that no permanent damage was inflicted to the cells during reoxygenation. These findings demonstrate the valuable applications of using MEA systems for modelling the dynamics of I/R injury in hiPSC-CMs over time, providing a platform for temporal resolution of pathogenesis at the functional level.

2. MiR-24-3p did not display cardioprotective effects, with no changes in functional activity of hiPSC-CMs transfected with miR-24-3p-specific mimics and inhibitors in any of the O_2 conditions. These findings were unexpected, due to the importance of its targets, such as *SCN5a* and *BIM*, in cardiac electrophysiology and cell death, respectively.

3. In a similar manner to the findings in hiPSC-CMs, miR-24-3p did not produce noteworthy changes in AC-16 CMs. However, as there were a few indications that BIM protein expression was reduced with the mimic and increased with the inhibitor from the Western blots, further work and optimization is warranted.

References

1. Global Health Estimates 2016: Deaths by Cause, Age, Sex, by Country and by Region, 2000-2016., World Health Organization, Geneva
2. Roth GA, Johnson C, Abajobir A, Abd-Allah F, Abera SF, et al. 2017. Global, Regional, and National Burden of Cardiovascular Diseases for 10 Causes, 1990 to 2015. *J Am Coll Cardiol* 70:1-25
3. O'Gara PT, Kushner FG, Ascheim DD, Casey DE, Jr., Chung MK, et al. 2013. 2013 ACCF/AHA guideline for the management of ST-elevation myocardial infarction: executive summary: a report of the American College of Cardiology Foundation/American Heart Association Task Force on Practice Guidelines. *J Am Coll Cardiol* 61:485-510
4. Jernberg T, Hasvold P, Henriksson M, Hjelm H, Thuresson M, Janzon M. 2015. Cardiovascular risk in post-myocardial infarction patients: nationwide real world data demonstrate the importance of a long-term perspective. *Eur Heart J* 36:1163-70
5. Thygesen K, Alpert JS, Jaffe AS, Chaitman BR, Bax JJ, et al. 2019. Fourth universal definition of myocardial infarction (2018). *Eur Heart J* 40:237-69
6. Bulluck H, Yellon DM, Hausenloy DJ. 2016. Reducing myocardial infarct size: challenges and future opportunities. *Heart* 102:341-8
7. Hausenloy DJ, Yellon DM. 2013. Myocardial ischemia-reperfusion injury: a neglected therapeutic target. *J Clin Invest* 123:92-100
8. Piper HM, Garcia-Dorado D, Ovize M. 1998. A fresh look at reperfusion injury. *Cardiovasc Res* 38:291-300
9. Eapen ZJ, Tang WH, Felker GM, Hernandez AF, Mahaffey KW, et al. 2012. Defining heart failure end points in ST-segment elevation myocardial infarction trials: integrating past experiences to chart a path forward. *Circ Cardiovasc Qual Outcomes* 5:594-600
10. Kalogeris T, Baines CP, Krenz M, Korthuis RJ. 2012. Cell biology of ischemia/reperfusion injury. *Int Rev Cell Mol Biol* 298:229-317
11. Heusch G, Gersh BJ. 2017. The pathophysiology of acute myocardial infarction and strategies of protection beyond reperfusion: a continual challenge. *Eur Heart J* 38:774-84
12. Kloner RA, Bolli R, Marban E, Reinlib L, Braunwald E. 1998. Medical and cellular implications of stunning, hibernation, and preconditioning: an NHLBI workshop. *Circulation* 97:1848-67
13. Manning AS, Hearse DJ. 1984. Reperfusion-induced arrhythmias: mechanisms and prevention. *J Mol Cell Cardiol* 16:497-518
14. Ito H. 2006. No-reflow phenomenon and prognosis in patients with acute myocardial infarction. *Nat Clin Pract Cardiovasc Med* 3:499-506
15. Jaffe R, Charron T, Puley G, Dick A, Strauss BH. 2008. Microvascular obstruction and the no-reflow phenomenon after percutaneous coronary intervention. *Circulation* 117:3152-6
16. Yellon DM, Hausenloy DJ. 2007. Myocardial reperfusion injury. *N Engl J Med* 357:1121-35
17. Pike MM, Luo CS, Clark MD, Kirk KA, Kitakaze M, et al. 1993. NMR measurements of Na+ and cellular energy in ischemic rat heart: role of Na(+)-H+ exchange. *Am J Physiol* 265:H2017-26
18. Sanada S, Komuro I, Kitakaze M. 2011. Pathophysiology of myocardial reperfusion injury: preconditioning, postconditioning, and translational aspects of protective measures. *Am J Physiol Heart Circ Physiol* 301:H1723-41

19. Griffiths EJ, Halestrap AP. 1995. Mitochondrial non-specific pores remain closed during cardiac ischaemia, but open upon reperfusion. *Biochem J* 307 (Pt 1):93-8
20. Lemasters JJ, Bond JM, Chacon E, Harper IS, Kaplan SH, et al. 1996. The pH paradox in ischemia-reperfusion injury to cardiac myocytes. *EXS* 76:99-114
21. Zweier JL, Talukder MA. 2006. The role of oxidants and free radicals in reperfusion injury. *Cardiovasc Res* 70:181-90
22. Davidson SM, Adameova A, Barile L, Cabrera-Fuentes HA, Lazou A, et al. 2020. Mitochondrial and mitochondrial-independent pathways of myocardial cell death during ischaemia and reperfusion injury. *J Cell Mol Med*
23. Kang PM, Izumo S. 2003. Apoptosis in heart: basic mechanisms and implications in cardiovascular diseases. *Trends Mol Med* 9:177-82
24. Galluzzi L, Bravo-San Pedro JM, Vitale I, Aaronson SA, Abrams JM, et al. 2015. Essential versus accessory aspects of cell death: recommendations of the NCCD 2015. *Cell Death Differ* 22:58-73
25. LeBlanc HN, Ashkenazi A. 2003. Apo2L/TRAIL and its death and decoy receptors. *Cell Death Differ* 10:66-75
26. Jin Z, El-Deiry WS. 2005. Overview of cell death signaling pathways. *Cancer Biol Ther* 4:139-63
27. Shi Y. 2002. Mechanisms of caspase activation and inhibition during apoptosis. *Mol Cell* 9:459-70
28. Hausenloy DJ, Yellon DM. 2015. Targeting Myocardial Reperfusion Injury--The Search Continues. *N Engl J Med* 373:1073-5
29. Colpaert RMW, Calore M. 2019. MicroRNAs in Cardiac Diseases. *Cells* 8
30. Gebert LFR, MacRae IJ. 2019. Regulation of microRNA function in animals. *Nat Rev Mol Cell Biol* 20:21-37
31. Lytle JR, Yario TA, Steitz JA. 2007. Target mRNAs are repressed as efficiently by microRNA-binding sites in the 5' UTR as in the 3' UTR. *Proc Natl Acad Sci U S A* 104:9667-72
32. Bartel DP. 2009. MicroRNAs: target recognition and regulatory functions. *Cell* 136:215-33
33. Friedman RC, Farh KK, Burge CB, Bartel DP. 2009. Most mammalian mRNAs are conserved targets of microRNAs. *Genome Res* 19:92-105
34. Lewis BP, Burge CB, Bartel DP. 2005. Conserved seed pairing, often flanked by adenosines, indicates that thousands of human genes are microRNA targets. *Cell* 120:15-20
35. Lewis BP, Shih IH, Jones-Rhoades MW, Bartel DP, Burge CB. 2003. Prediction of mammalian microRNA targets. *Cell* 115:787-98
36. Lee Y, Kim M, Han J, Yeom KH, Lee S, et al. 2004. MicroRNA genes are transcribed by RNA polymerase II. *EMBO J* 23:4051-60
37. Ha M, Kim VN. 2014. Regulation of microRNA biogenesis. *Nat Rev Mol Cell Biol* 15:509-24
38. Bartel DP. 2004. MicroRNAs: genomics, biogenesis, mechanism, and function. *Cell* 116:281-97
39. Carthew RW, Sontheimer EJ. 2009. Origins and Mechanisms of miRNAs and siRNAs. *Cell* 136:642-55
40. Lee Y, Ahn C, Han J, Choi H, Kim J, et al. 2003. The nuclear RNase III Drosha initiates microRNA processing. *Nature* 425:415-9
41. Han J, Lee Y, Yeom KH, Kim YK, Jin H, Kim VN. 2004. The Drosha-DGCR8 complex in primary microRNA processing. *Genes Dev* 18:3016-27
42. Kobayashi H, Tomari Y. 2016. RISC assembly: Coordination between small RNAs and Argonaute proteins. *Biochim Biophys Acta* 1859:71-81
43. Treiber T, Treiber N, Meister G. 2018. Author Correction: Regulation of microRNA biogenesis and its crosstalk with other cellular pathways. *Nat Rev Mol Cell Biol* 19:808
44. Chen JF, Murchison EP, Tang R, Callis TE, Tatsuguchi M, et al. 2008. Targeted deletion of Dicer in the heart leads to dilated cardiomyopathy and heart failure. *Proc Natl Acad Sci U S A* 105:2111-6

45. Singh MK, Lu MM, Massera D, Epstein JA. 2011. MicroRNA-processing enzyme Dicer is required in epicardium for coronary vasculature development. *J Biol Chem* 286:41036-45
46. Ghai V, Wang K. 2016. Recent progress toward the use of circulating microRNAs as clinical biomarkers. *Arch Toxicol* 90:2959-78
47. Ovchinnikova ES, Schmitter D, Vegter EL, Ter Maaten JM, Valente MA, et al. 2016. Signature of circulating microRNAs in patients with acute heart failure. *Eur J Heart Fail* 18:414-23
48. Pan LJ, Wang X, Ling Y, Gong H. 2017. MiR-24 alleviates cardiomyocyte apoptosis after myocardial infarction via targeting BIM. *Eur Rev Med Pharmacol Sci* 21:3088-97
49. Qian L, Van Laake LW, Huang Y, Liu S, Wendland MF, Srivastava D. 2011. miR-24 inhibits apoptosis and represses Bim in mouse cardiomyocytes. *J Exp Med* 208:549-60
50. Strasser A, Cory S, Adams JM. 2011. Deciphering the rules of programmed cell death to improve therapy of cancer and other diseases. *EMBO J* 30:3667-83
51. Chipuk JE, Moldoveanu T, Llambi F, Parsons MJ, Green DR. 2010. The BCL-2 family reunion. *Mol Cell* 37:299-310
52. Danial NN, Korsmeyer SJ. 2004. Cell death: critical control points. *Cell* 116:205-19
53. Riedl SJ, Salvesen GS. 2007. The apoptosome: signalling platform of cell death. *Nat Rev Mol Cell Biol* 8:405-13
54. Li DF, Tian J, Guo X, Huang LM, Xu Y, et al. 2012. Induction of microRNA-24 by HIF-1 protects against ischemic injury in rat cardiomyocytes. *Physiol Res* 61:555-65
55. Takahashi K, Tanabe K, Ohnuki M, Narita M, Ichisaka T, et al. 2007. Induction of pluripotent stem cells from adult human fibroblasts by defined factors. *Cell* 131:861-72
56. Paik DT, Chandy M, Wu JC. 2020. Patient and Disease-Specific Induced Pluripotent Stem Cells for Discovery of Personalized Cardiovascular Drugs and Therapeutics. *Pharmacol Rev* 72:320-42
57. Shi Y, Inoue H, Wu JC, Yamanaka S. 2017. Induced pluripotent stem cell technology: a decade of progress. *Nat Rev Drug Discov* 16:115-30
58. 2018. *Stem cell genetics for biomedical research : past, present, and future*. New York, NY: Springer Science+Business Media. pages cm pp.
59. Doss MX, Sachinidis A. 2019. Current Challenges of iPSC-Based Disease Modeling and Therapeutic Implications. *Cells* 8
60. Davidson MM, Nesti C, Palenzuela L, Walker WF, Hernandez E, et al. 2005. Novel cell lines derived from adult human ventricular cardiomyocytes. *J Mol Cell Cardiol* 39:133-47
61. Burridge PW, Holmstrom A, Wu JC. 2015. Chemically Defined Culture and Cardiomyocyte Differentiation of Human Pluripotent Stem Cells. *Curr Protoc Hum Genet* 87:21 3 1- 3 15
62. Lian X, Zhang J, Azarin SM, Zhu K, Hazeltine LB, et al. 2013. Directed cardiomyocyte differentiation from human pluripotent stem cells by modulating Wnt/beta-catenin signaling under fully defined conditions. *Nat Protoc* 8:162-75
63. FDA. 2019. *Novel Drug Approvals for 2018*. https://www.fda.gov/drugs/new-drugs-fda-cders-new-molecular-entities-and-new-therapeutic-biological-products/novel-drug-approvals-2018
64. Sayed N, Liu C, Wu JC. 2016. Translation of Human-Induced Pluripotent Stem Cells: From Clinical Trial in a Dish to Precision Medicine. *J Am Coll Cardiol* 67:2161-76
65. Chen IY, Matsa E, Wu JC. 2016. Induced pluripotent stem cells: at the heart of cardiovascular precision medicine. *Nat Rev Cardiol* 13:333-49
66. Kussauer S, David R, Lemcke H. 2019. hiPSCs Derived Cardiac Cells for Drug and Toxicity Screening and Disease Modeling: What Micro- Electrode-Array Analyses Can Tell Us. *Cells* 8

67. Nozaki Y, Honda Y, Watanabe H, Saiki S, Koyabu K, et al. 2016. CSAHi study: Validation of multi-electrode array systems (MEA60/2100) for prediction of drug-induced proarrhythmia using human iPS cell-derived cardiomyocytes -assessment of inter-facility and cells lot-to-lot-variability. *Regul Toxicol Pharmacol* 77:75-86
68. Goineau S, Castagne V. 2018. Electrophysiological characteristics and pharmacological sensitivity of two lines of human induced pluripotent stem cell derived cardiomyocytes coming from two different suppliers. *J Pharmacol Toxicol Methods* 90:58-66
69. Kozomara A, Birgaoanu M, Griffiths-Jones S. 2019. miRBase: from microRNA sequences to function. *Nucleic Acids Res* 47:D155-D62
70. Livak KJ, Schmittgen TD. 2001. Analysis of relative gene expression data using real-time quantitative PCR and the 2(-Delta Delta C(T)) Method. *Methods* 25:402-8
71. Ye J, Coulouris G, Zaretskaya I, Cutcutache I, Rozen S, Madden TL. 2012. Primer-BLAST: a tool to design target-specific primers for polymerase chain reaction. *BMC Bioinformatics* 13:134
72. Wang X, Spandidos A, Wang H, Seed B. 2012. PrimerBank: a PCR primer database for quantitative gene expression analysis, 2012 update. *Nucleic Acids Res* 40:D1144-9
73. Pradhapan P, Kuusela J, Viik J, Aalto-Setala K, Hyttinen J. 2013. Cardiomyocyte MEA data analysis (CardioMDA)--a novel field potential data analysis software for pluripotent stem cell derived cardiomyocytes. *PLoS One* 8:e73637
74. Tertoolen LGJ, Braam SR, van Meer BJ, Passier R, Mummery CL. 2018. Interpretation of field potentials measured on a multi electrode array in pharmacological toxicity screening on primary and human pluripotent stem cell-derived cardiomyocytes. *Biochem Biophys Res Commun* 497:1135-41
75. Shimoda LA, Polak J. 2011. Hypoxia. 4. Hypoxia and ion channel function. *Am J Physiol Cell Physiol* 300:C951-67
76. Garcia-Dorado D, Ruiz-Meana M, Inserte J, Rodriguez-Sinovas A, Piper HM. 2012. Calcium-mediated cell death during myocardial reperfusion. *Cardiovasc Res* 94:168-80
77. Wang R, Wang M, He S, Sun G, Sun X. 2020. Targeting Calcium Homeostasis in Myocardial Ischemia/Reperfusion Injury: An Overview of Regulatory Mechanisms and Therapeutic Reagents. *Front Pharmacol* 11:872
78. Priori SG, Mantica M, Napolitano C, Schwartz PJ. 1990. Early afterdepolarizations induced in vivo by reperfusion of ischemic myocardium. A possible mechanism for reperfusion arrhythmias. *Circulation* 81:1911-20
79. Stowe DF. 1999. Understanding the temporal relationship of ATP loss, calcium loading, and rigor contracture during anoxia, and hypercontracture after anoxia in cardiac myocytes. *Cardiovasc Res* 43:285-7
80. Siegmund B, Schlack W, Ladilov YV, Balser C, Piper HM. 1997. Halothane protects cardiomyocytes against reoxygenation-induced hypercontracture. *Circulation* 96:4372-9
81. Abdallah Y, Gkatzoflia A, Gligorievski D, Kasseckert S, Euler G, et al. 2006. Insulin protects cardiomyocytes against reoxygenation-induced hypercontracture by a survival pathway targeting SR Ca2+ storage. *Cardiovasc Res* 70:346-53
82. Garcia-Dorado D, Piper HM, Eisner DA. 2008. Sarcoplasmic reticulum and mitochondria in cardiac pathophysiology. *Cardiovasc Res* 77:231-3
83. Piper HM, Kasseckert S, Abdallah Y. 2006. The sarcoplasmic reticulum as the primary target of reperfusion protection. *Cardiovasc Res* 70:170-3
84. Walsh JG, Logue SE, Luthi AU, Martin SJ. 2011. Caspase-1 promiscuity is counterbalanced by rapid inactivation of processed enzyme. *J Biol Chem* 286:32513-24
85. Zhang X, Yoon JY, Morley M, McLendon JM, Mapuskar KA, et al. 2018. A common variant alters SCN5A-miR-24 interaction and associates with heart failure mortality. *J Clin Invest* 128:1154-63

86. Luo X, Zhang H, Xiao J, Wang Z. 2010. Regulation of human cardiac ion channel genes by microRNAs: theoretical perspective and pathophysiological implications. *Cell Physiol Biochem* 25:571-86
87. de Lera Ruiz M, Kraus RL. 2015. Voltage-Gated Sodium Channels: Structure, Function, Pharmacology, and Clinical Indications. *J Med Chem* 58:7093-118
88. Gintant GA, Gallacher DJ, Pugsley MK. 2011. The 'overly-sensitive' heart: sodium channel block and QRS interval prolongation. *Br J Pharmacol* 164:254-9
89. Fabian MR, Sonenberg N, Filipowicz W. 2010. Regulation of mRNA translation and stability by microRNAs. *Annu Rev Biochem* 79:351-79
90. Jin Y, Chen Z, Liu X, Zhou X. 2013. Evaluating the microRNA targeting sites by luciferase reporter gene assay. *Methods Mol Biol* 936:117-27
91. Liu J, Carmell MA, Rivas FV, Marsden CG, Thomson JM, et al. 2004. Argonaute2 is the catalytic engine of mammalian RNAi. *Science* 305:1437-41
92. Chendrimada TP, Finn KJ, Ji X, Baillat D, Gregory RI, et al. 2007. MicroRNA silencing through RISC recruitment of eIF6. *Nature* 447:823-8
93. Pillai RS, Bhattacharyya SN, Artus CG, Zoller T, Cougot N, et al. 2005. Inhibition of translational initiation by Let-7 MicroRNA in human cells. *Science* 309:1573-6
94. Petersen CP, Bordeleau ME, Pelletier J, Sharp PA. 2006. Short RNAs repress translation after initiation in mammalian cells. *Mol Cell* 21:533-42
95. Guo H, Ingolia NT, Weissman JS, Bartel DP. 2010. Mammalian microRNAs predominantly act to decrease target mRNA levels. *Nature* 466:835-40
96. Eichhorn SW, Guo H, McGeary SE, Rodriguez-Mias RA, Shin C, et al. 2014. mRNA destabilization is the dominant effect of mammalian microRNAs by the time substantial repression ensues. *Mol Cell* 56:104-15
97. Djuranovic S, Nahvi A, Green R. 2012. miRNA-mediated gene silencing by translational repression followed by mRNA deadenylation and decay. *Science* 336:237-40
98. Bazzini AA, Lee MT, Giraldez AJ. 2012. Ribosome profiling shows that miR-430 reduces translation before causing mRNA decay in zebrafish. *Science* 336:233-7
99. Holly TA, Drincic A, Byun Y, Nakamura S, Harris K, et al. 1999. Caspase inhibition reduces myocyte cell death induced by myocardial ischemia and reperfusion in vivo. *J Mol Cell Cardiol* 31:1709-15
100. Huang JQ, Radinovic S, Rezaiefar P, Black SC. 2000. In vivo myocardial infarct size reduction by a caspase inhibitor administered after the onset of ischemia. *Eur J Pharmacol* 402:139-42
101. Yaoita H, Ogawa K, Maehara K, Maruyama Y. 1998. Attenuation of ischemia/reperfusion injury in rats by a caspase inhibitor. *Circulation* 97:276-81
102. Fiedler J, Jazbutyte V, Kirchmaier BC, Gupta SK, Lorenzen J, et al. 2011. MicroRNA-24 regulates vascularity after myocardial infarction. *Circulation* 124:720-30